Hypocretin/orexin neurons encode social discrimination and exhibit a sex-dependent necessity for social interaction

Author Names and Affiliations:

Matthew Dawson[1,5,6], Dylan J Terstege[3,4,5], Naila Jamani[1,5,6], Mio Tsutsui[1,5,6], Dmitrii Pavlov[1,5,6], Raluca Bugescu[7], Jonathan R Epp[3,4,5], Gina M Leinninger[7], Derya Sargin[1,2,5,6]

Department of Psychology[1], Department of Physiology & Pharmacology[2], Department of Cell Biology and Anatomy[3], Cumming School of Medicine[4], Hotchkiss Brain Institute[5], Alberta Children's Hospital Research Institute[6], University of Calgary, Canada

Department of Physiology[7], Michigan State University, United States

Corresponding author:

Derya Sargin

Address:

University of Calgary

2500 University Ave Dr NW T2N 1N4

Calgary, AB, Canada

Phone: 403-2204349

Email: derya.sargin@ucalgary.ca

Summary

Intraspecies social interactions are integral for survival and maintenance of society among all mammalian species. Yet, our understanding of the neural systems and mechanisms involved in the establishment of social connectedness are limited. Since their initial discovery as regulators of sleep/wakefulness and appetite in the brain, the hypocretin/orexin neurons have also been shown to play an essential role in modulating energy homeostasis, motivated and emotional behavior. These neurons are located exclusively in the hypothalamus which, regulates complex and goal-directed behaviors. The hypothalamus also plays an important role in the modulation of social behavior by encoding internal states. However, our understanding of the role of hypocretin neurons in social behavior is currently limited. To address this knowledge gap, we performed a combination of fiber photometry and machine learning based behavioral analysis in female and male mice expressing GCaMP6s in hypocretin neurons. We then applied optogenetic and pharmacological inhibition of hypocretin neuron signaling to determine the necessity of the hcrt neuron population for social behavior. Our results indicate that hypocretin neurons exhibit a robust increase in activity in response to social interaction in both female and male mice. We show here for the first time a social discrimination signal that is encoded differentially by hcrt neurons based on the nature of the social encounter. The intensity of the hcrt neuron activity predicts the subsequent duration of social interaction. The optogenetic inhibition of hypocretin neuron activity during social behavior leads to a reduction in the amount of time mice are engaged in social interaction in males but not in females. Blocking hcrt1 (orexin 1) receptors similarly reduces social interaction in males only. Reduced hcrt1 receptor signaling results in increased activity in the insular cortex and reduced activity in the VTA after social interaction in male mice. Together, these data implicate the lateral hypothalamus hypocretin neurons as a sexually dimorphic key regulator within the larger network of neural systems involved in social behavior. Our findings carry significant implications for the treatment of neuropsychiatric diseases characterized by

social dysfunction, particularly considering the varying prevalence observed across different sexes.

Introduction

Social behaviors are an essential component of survival for most organisms. Effectively and appropriately communicating with members of one's species enables an individual to gain access to information about foraging opportunities, potential mates and detection of threats. Interactions between conspecifics also provide the foundation for social group hierarchies, providing members with protection from predation, support from others within the group, and obtaining emotional rewards. The importance of these gains for the success of an organism has led to lasting evolutionary conservation of social behaviors, over time reinforcing the development of complex neural systems for the more sophisticated and refined methods of social interaction we see in mammals.

For organisms to interact socially, each must collect and process sensory signals from their counterparts and their environment, integrate this information with their internal state (e.g., memories of prior experiences, affective state, evaluation of risks and rewards), determine the appropriate behavioral response for the situation, then perform a sequence of corresponding motor patterns. These processes must function in concert simultaneously and rapidly to accommodate the highly dynamic and unpredictable process of social interaction (Chen and Hong, 2018). The resulting neural networks required to orchestrate this are vast, and we are still early in our understanding of which anatomical regions of the brain are involved and what their individual contribution to social behaviors is. Despite the challenge inherent to elucidating the underlying mechanisms of such complicated behaviors, many recent studies have made significant advances in our understanding of the neural substrates of social behaviors. Research in rodent models has demonstrated the involvement of numerous cortical and subcortical regions in production and direction of social behavior (Anderson, 2016; Clancy et al., 1984; Gunaydin et

al., 2014; Hashikawa et al., 2016; Y. Hashikawa et al., 2017; Hofer, 1996; Hong et al., 2014; Keller et al., 2006; Kingsbury et al., 2019; Li et al., 2016; Marlin et al., 2015; Okuyama, 2018; Takahashi et al., 2014; Unger et al., 2015; Veening and Coolen, 2014; Wei et al., 2021). These regions have been found to form extensive functional circuits between each other and work to govern the array of parallel processes required during social interaction.

The various regions of the hypothalamus play a particularly important role in the modulation of social behavior by encoding internal states (Lo et al., 2019). The evolutionarily conserved hypothalamus (Xie and Dorsky, 2017) regulates critical survival functions by processing sensory and neuroendocrine signals and producing internal states to promote the organism to adjust its behavior to maintain homeostasis (Saper and Lowell, 2014). Certain internal states including emotion, memories of past experiences, motivation, and arousal are critical mediators in social behaviors as they determine the appropriate behavioral expression in response to incoming sensory information (Anderson, 2016). The modulatory power of these internal states over the social behavior of an animal is immense, to the degree that identical sensory stimuli and environmental conditions can elicit completely different behavioral responses based on the animal's internal state (Chen and Hong, 2018). A shared underlying characteristic to all these internal states is that behavioral arousal is required to produce attention to socially relevant signals and motivation to investigate and interact with the conspecific from which they originate. This systemic arousal directed towards social stimuli is a process central to social behavior and closely overlaps with the functional role of the lateral hypothalamus (LH). Since their discovery (de Lecea et al., 1998; Sakurai et al., 1998), the LH hypocretin (hcrt)/ orexin neurons have been shown to govern arousal (Bourgin et al., 2000; Del Cid-Pellitero and Garzón, 2011; Hasegawa et al., 2017, 2014; Yang et al., 2019), attentional (Fadel and Burk, 2010; Fadel and Frederick-Duus, 2008), and motivational (España et al., 2011, 2010; Fadel and Deutch, 2002; Vittoz et al., 2008) states which all contribute to modulation of social behavior. Hcrt neurons extensively project to and modulate the activity of brain regions involved in social interaction

103 (Bisetti et al., 2006; Lungwitz et al., 2012; Samson et al., 2002; Sterley et al., 2018), social reward
104 (Fadel and Deutch, 2002; Gunaydin et al., 2014; Payet et al., 2021; Wang et al., 2005), and social
105 memory (Yang et al., 2013). However, their direct role in social behavior has been less studied.

106 To reveal how hcrt neuron activity contribute to social behavior, we employed Cre-
107 inducible viral targeting combined with fiber photometry and optogenetic tools in *Hcrt*$^{IRES\text{-}Cre}$ mice
108 during conspecific social interactions. We identified that hcrt neurons exhibit a robust increase in
109 activity in response to social interaction. We demonstrate that hcrt neuron activity is more
110 pronounced during interaction between unfamiliar mice compared to that observed during familiar
111 interactions. In contrast, exposing mice to familiar or novel objects does not lead to a difference
112 in the activity of hcrt neurons suggesting that differential activity is driven primarily by social
113 interactions. We further found that social interaction recruits a larger proportion of hcrt neurons in
114 males, compared with females. The acute optogenetic inhibition of hcrt neuron activity and
115 reducing hcrt signaling by blocking hcrt-1 receptors during social behavior disrupts social
116 interaction in male mice without an effect in females. In males, we detected increased insular
117 cortex and reduced VTA activity in mice injected with the hcrt-1 antagonist and subjected to social
118 interaction. Together, our data compelling evidence for the sex-dependent role for hcrt neurons
119 and downstream postsynaptic regions in social behavior.

120 **Results**

121 **The activity of the LH hcrt neuron population increases in response to social investigation.**
122 To monitor the activity of hcrt neuron population in response to social approach and investigation,
123 we used fiber photometry while performing a 3-chamber sociability test (Moy et al., 2004). We
124 infused a Cre-dependent adeno-associated virus (AAV) encoding the fluorescent sensor
125 GCaMP6s into the LH of *Hcrt*$^{IRES\text{-}Cre}$ mice. We found that >90 % of virus-labeled cells co-
126 expressed Hcrt, while 58 % Hcrt+ cells were transduced with the virus (**Figure 1A, B; Figure S1,**
127 **S2**), similar to the previously published *Hcrt-cre* knock-in lines (Giardino et al., 2018; Mitchell et
128 al., 2020). An optical fiber was implanted above the LH to allow the delivery of excitation light and

129 collection of GCaMP6s fluorescence from hcrt neurons specifically (**Figure 1A, B**). After 5 min
130 baseline recording in the middle zone of the 3-chamber apparatus, mice were given access to
131 freely explore the chamber containing a confined social target (age and sex-matched novel
132 conspecific) in one chamber and an empty non-social zone in other chamber (**Figure 1C**). We
133 first averaged the hcrt Ca^{2+} signals in response to the social interaction that occurred within 2 sec
134 of the social zone entrance and compared this with the Ca^{2+} signals in mice during their interaction
135 with the empty cup in the non-social zone. 2 sec duration after entrance was selected restrict our
136 analysis to the bouts in which mice directly visited the sniffing zones after entering the chamber.
137 In female mice, the hcrt neuron activity increased after entering the social and non-social zones
138 (t>0 sec) and during interaction in the sniffing zones however, the activity between social and
139 non-social zones remained non-significant (two-way ANOVA; effect of time: $F(2, 18) = 15.96$, $p <$
140 0.001, effect of zone: $F(1, 18) = 0.07$, $p = 0.79$) (**Figure 1D, E**). The area under the curve of the
141 averaged hcrt Ca^{2+} responses were similar whether the female mice entered the social zone or
142 the non-social zone (paired t-test; $p = 0.96$) (**Figure 1F**). In male mice, the hcrt Ca^{2+} response
143 started to increase within 1 sec prior to and reached maximum levels right after entrance into the
144 social zone (**Figure 1G**). The hcrt Ca^{2+} response in male mice was significantly larger during and
145 after entrance into the social zone when compared with the non-social zone (two-way ANOVA;
146 effect of time: $F(2, 24) = 12.86$, $p = 0.0002$, effect of zone: $F(1,24) = 11.2$, $p = 0.0027$) (**Figure**
147 **1H**). The area under the curve of the averaged hcrt Ca^{2+} responses was significantly larger when
148 male mice entered the social zone rather than the non-social zone (*paired t-test; $p = 0.025$)
149 (**Figure 1I**).

150 We next compared the difference in the activity of hcrt neuron population while mice were
151 actively sniffing the confined conspecific (social sniffing zone) or the empty cup (non-social
152 sniffing zone) (**Figure 1J**). During interaction with the social target, hcrt Ca^{2+} response was
153 significantly larger regardless of sex (two-way ANOVA; effect of zone: $F(1, 14) = 6.55$, $p = 0.023$,
154 effect of sex: $F(1, 14) = 4.56$, $p = 0.051$) when compared to the time spent in the non-social sniffing

155 zone (**Figure 1K**). Further analysis of the data using planned comparisons between social and
156 non-social sniffing zones revealed that hcrt Ca^{2+} response was significantly larger in the social
157 sniffing zone, compared with the non-social sniffing zone in males, but not in females (Fisher's
158 LSD; social vs non-social: females, p = 0.69, males, p = 0.004) (**Figure 1K**). The frequency of
159 activity (peaks/sec) during interaction with the social target was significantly higher compared to
160 the non-social interaction, with females having an overall greater frequency (two-way ANOVA;
161 effect of zone: $F(1, 14) = 7.77$, $p = 0.014$, effect of sex: $F(1, 14) = 9.15$, $p = 0.009$). Planned
162 comparisons of the frequency between social and non-social sniffing zones revealed a significant
163 difference for males but not females (Fisher's LSD; social vs non-social: females, p = 0.16, males,
164 p = 0.024) (**Figure 1L**). The area under the curve of the hcrt Ca^{2+} signal changes was significantly
165 larger when male mice interacted with the social target compared to the interaction in the non-
166 social sniffing zone. This difference was not significant in females (two-way ANOVA; zone X sex
167 interaction: $F(1, 14) = 6.74$, $p = 0.021$; Tukey's multiple comparisons test: Social vs non-social
168 sniffing zone; Males $^{**}p = 0.006$, females $p = 0.99$) (**Figure 1M**).

169 Taken together, our data show that the response of the hcrt neuron population is larger
170 when mice are actively sniffing the social conspecific when compared with the non-social
171 exploration of an empty cup. This response is more prominent in males when they enter the social
172 zone and interact with the social target, compared to females. However, regardless of sex, mice
173 show an overall higher hcrt activity during the time they spent actively interacting with the social
174 target in the sniffing zone.

175 **Differential activity in the LH hcrt neuron population in response to familiar and novel**
176 **social interaction.** While the 3-chamber sociability test allows exploration of social interaction
177 within a controlled setting, it does not allow direct social interaction. To determine the changes in
178 the activity of hcrt neuron population during reciprocal and active social interaction, we performed
179 fiber photometry in the resident mice while they are socially interacting in their home cage.
180 Accordingly, we performed 5 min baseline recordings after which the resident mouse is first

181 introduced to a cage partner (familiar conspecific) and allowed to interact for 5 min. After removing
182 the familiar conspecific from the cage followed by a 5 min additional baseline recording, the
183 resident mouse was introduced to a novel age-, sex- and strain-matched conspecific (stranger)
184 and allowed to interact for 5 min (**Figure 2A**). This order was selected due to the possibility that
185 potentially aggressive encounters with the stranger mice would increase the stress levels and
186 confound subsequent interaction with a familiar mouse. In addition, the behavior of the familiar
187 mouse towards the experimental mouse could be influenced by the odor of a previous stranger.
188 To rule out the possibility of habituation, we determined changes in the hcrt neuron activity during
189 subsequent interactions. We did not detect a difference in the hcrt neuron activity in the resident
190 mouse when a familiar or a stranger mouse was introduced twice in a row (**Figure S3**). In the
191 home cage, social interaction was initiated exclusively by the resident mouse approaching the
192 mouse introduced into the cage (Fam: 1.41 ± 0.23 sec, Stranger: 1.6 ± 0.55 sec after introduction).
193 Social approach was defined as the time the resident mouse initiated movement toward the social
194 target (Gunaydin et al., 2014). Averaging the hcrt Ca^{2+} signals over time in both female and male
195 mice showed that the hcrt activity in resident mice started to increase prior to initial approach,
196 reached maximum levels right after the initial approach and sniffing and returned to baseline
197 minutes after the first interaction (**Figure 2B, C**). The analysis of the area under the curve of the
198 averaged hcrt Ca^{2+} traces showed that the hcrt Ca^{2+} response was significantly larger in female
199 and male resident mice during interaction with the unfamiliar conspecifics compared to the
200 interaction with the familiar cage mates (two-way ANOVA; effect of conspecific: $F(1, 26) = 8.96$,
201 $p = 0.006$, effect of sex: $F(1, 26) = 1.78$, $p = 0.19$). Planned comparisons between familiar and
202 stranger interactions revealed a significant difference in males but not in females (Fisher's LSD;
203 familiar vs stranger: females, $p = 0.1$, males, $p = 0.016$) (**Figure 2D, E**). The maximum hcrt activity
204 (max z-score $\Delta F/F$) within 10 sec of initial approach was significantly greater during interaction
205 between unfamiliar (resident and stranger) compared to that observed during familiar interactions
206 in both female and male mice, with activity being larger during both types of social interaction in

male mice compared with female mice (two-way ANOVA; effect of conspecific: $F(1, 26) = 8.01$, $p = 0.009$, effect of sex: $F(1, 26) = 8.29$, $p = 0.008$). Planned comparisons revealed a significant difference in females (Fisher's LSD; familiar vs stranger: females, $p = 0.03$, males, $p = 0.09$) (**Figure 2F**). We did not detect a difference in variances between females and males (Levene's test; z-score; $F(3, 26) = 1.11$, $p = 0.36$). The social novelty index did not differ between the sexes (mean ± SEM: Males, 0.21 ± 0.08; Females, 0.22 ± 0.1; unpaired t-test, $t = 0.32$, df = 13, $p = 0.97$).

Next, we sought to determine the interaction between the initial large increase in hcrt activity with social behavior. We found a significant correlation between the first interaction-induced maximum hcrt activity and the time the resident mice spent sniffing the stranger mice (interaction %) within the subsequent 5 min of the social behavior task (Stranger: $r(13) = 0.58$, $^*p = 0.023$, Familiar: $r(13) = 0.37$, $p = 0.18$) **(Figure 2G)**. To further determine the relation between the hcrt signal and social behavior, we plotted the maximum hcrt activity (**Figure 2H**) along with the duration of the time spent by the resident mice sniffing the conspecifics (**Figure 2I**) over time. These data have been analyzed by three-way ANOVA with sex and conspecific as factors and time as a repeated measure. The maximum hcrt activity was the greatest during the first minute after mice met for the first time and declined over the subsequent minutes of the task (effect of time: $F(14, 364) = 21.26$, $p < 0.001$). This was found to be dependent on both sex (time X sex interaction: $F(14, 364) = 2.19$, $p = 0.007$; Tukey's multiple comparisons test: Male vs female at 20 sec $p = 0.013$, 40 sec $p = 0.033$, all other time points *p's* > 0.05), and conspecific (time X conspecific interaction: $F(14, 364) = 2.32$, $p = 0.004$; Tukey's multiple comparisons test: Stranger vs familiar at 20 sec $p = 0.035$, 40 sec $p = 0.009$, all other time points *p's* > 0.05) (**Figure 2H, I**) suggesting the engagement of this neuron population during initial contact. The time spent sniffing was significantly greater in males than females (effect of sex: $F(1, 26) = 4.62$, $p = 0.041$). Both female and male mice spent a significantly greater time sniffing the stranger mice compared with familiar cage mates (effect of conspecific: $F(1, 26) = 11.81$, $p = 0.002$). Similar to the decrease

233 in the hcrt activity, the initial difference in the time spent sniffing the stranger and familiar mice
234 declined over time (time X conspecific interaction: $F(14, 364) = 3.46$, $p < 0.001$, Tukey's multiple
235 comparisons test: Stranger vs familiar at 40 sec $p < 0.001$, 60 sec $p = 0.0013$, 80 sec $p = 0.005$
236 all other time points *p's* > 0.05).

237 The greater social interaction-induced hcrt activity increase in males may depend on a
238 larger number of neurons infected, when compared with females. To determine this, we
239 performed immunohistochemistry for GFP and quantified the number of hcrt cells expressing
240 GCaMP6s in both sexes. We found no significant difference in the number of GFP+ hcrt neurons
241 infused with AAV encoding GCaMP6s (unpaired t-test, $t = 1.05$, $df = 10$, $p = 0.32$) (**Figure S4A,**
242 **B**). We next hypothesized that the amount of hcrt neurons recruited by the initial interaction may
243 be different between females and males. To further investigate this, we perfused mice 90 min
244 after social interaction with a stranger conspecific and analyzed the percentage of hcrt neurons
245 expressing cFos in both sexes. We found that the amount of hcrt neurons expressing cFos after
246 social interaction was significantly larger in male mice, compared with females (unpaired t-test, t
247 = 3.56, df = 6, $p = 0.012$) (**Figure S4C, D**). In contrast, we did not detect a difference in the number
248 of hcrt neurons between females and males (unpaired t-test, $t = 0.34$, $df = 6$, $p = 0.74$) (**Figure**
249 **S4E**).

250 Overall, these data show that hcrt neuron activity plays a significant and differential role in
251 social interaction. We provide the first evidence that unfamiliar mice evoke a greater response in
252 hcrt neuron activity than familiar mice. The peak hcrt signal induced by the initial approach and
253 sniffing determines the subsequent time of interaction between the unfamiliar animals. Both
254 female and male mice show an increase hcrt activity in response to stranger interaction compared
255 with familiar however, male mice show greater hcrt activity and sniffing behavior regardless of the
256 conspecific. Moreover, males have a greater percentage of hcrt neurons that are activated in
257 response to social interaction, as indicated by elevated cFos levels compared with females.

258 **Differential hcrt neuron activity during social interaction persists in the novel cage but**
259 **absent in response to object investigation.** The choice of the home cage social interaction
260 assay for our experiments allowed us to assess social interaction within the territorial environment
261 of the resident mice. To determine whether the greater hcrt signal to a stranger conspecific
262 persists in a non-territorial novel setting, we placed the experimental mice in a cage with novel
263 bedding and performed fiber photometry during interaction with familiar and stranger mice (**Figure**
264 **3A**). In a novel cage, mice spent significantly more time engaging in non-social behaviors
265 including rearing, ambulation and grooming compared to those in the home cage (**Figure S5A**).
266 However, the time mice spent interacting with the familiar or the stranger conspecific was
267 comparable in both cages (**Figure S5B-S5D**).

268 Similar to our observations in the home cage, the increase in the hcrt Ca^{2+} signal reached
269 maximum levels in female and male mice right after the first approach and sniffing in the novel
270 cage (**Figure 3B, C**). The quantification of the area under the curve of the averaged hcrt Ca^{2+}
271 traces revealed a greater hcrt activity when mice interacted with a stranger compared to a familiar
272 mouse (two-way ANOVA; effect of conspecific: $F(1, 18) = 4.91$, $p = 0.038$) (**Figure 3D**). The
273 maximum hcrt activity (max z-score $\Delta F/F$) within 10 sec of initial approach was also significantly
274 greater when mice interacted with a stranger compared with a familiar mouse (two-way ANOVA;
275 effect of conspecific: $F(1, 18) = 19.14$, $p = 0.0004$). The hcrt activity was significantly larger in
276 male mice during interaction with both familiar and stranger mice, when compared with females
277 (two-way ANOVA; effect of sex: $F(1, 18) = 4.87$, $p = 0.041$). Planned comparisons between
278 familiar and stranger interactions revealed a significant difference for both females and males
279 (Fisher's LSD; familiar vs stranger: females, $p = 0.006$, males, $p = 0.006$) (**Figure 3E**), and was
280 comparable to the signal observed during interaction in the home cage (**Figure S5E, F**). Similar
281 to the home cage setting, the initial interaction-induced maximum hcrt activity correlated with the
282 amount of interaction with the stranger conspecifics (**Figure 3F**). We did not detect a difference
283 in variances between females and males (Levene's test; z-score; $F(3, 18) = 3.32$, $p = 0.3$). Social

284 novelty index also did not differ females and males (mean ± SEM: Males, 0.17 ± 0.05; Females,
285 0.23 ± 0.07; unpaired t-test, t = 0.61, df = 9, p = 0.55). Altogether, these data show that the activity
286 of hcrt neuron population is greater while mice are engaged with stranger conspecifics whether
287 they are in their territorial home cage environment or in a novel cage, with higher hcrt activity and
288 sniffing behavior in males in both settings.

289 To identify whether the differential activity in the hcrt neuron population is a general
290 response to novelty or specific to social interaction, we performed fiber photometry while mice
291 were exposed to a familiar or a novel object in their home cage. Experimental mice were pre-
292 exposed to the familiar object for at least 3 days in their home cage (Okuyama et al., 2016). In
293 this task, we presented the experimental mice with a familiar or a novel object following a 5 min
294 baseline recording (**Figure 3G**). In both female and male mice, we observed an increase in the
295 hcrt Ca^{2+} signal in response to initial approach and interaction with the objects (**Figure 3H**). In
296 contrast to the differential hcrt signal observed during familiar and stranger mouse interactions,
297 both the maximum hcrt Ca^{2+} signal and the area under the curve for the first 2 min of interaction
298 were similar during novel and familiar object interactions (**Figure 3I, J**). This showed that the
299 significant difference in the hcrt Ca^{2+} signal during social interaction was absent when mice
300 interacted with the familiar or novel objects, suggesting that the differential activity is specific to
301 social interaction.

302 Because female and male mice employ different strategies (Anderson, 2016; van den
303 Berg et al., 2015), we further analyzed the two distinct modalities of social investigative behaviors
304 that the experimental mice engaged in, including anogenital sniffing (examination of the
305 anogenital area of the conspecific) and the head/torso sniffing (examination of the head and torso
306 region of the conspecific (Lee et al., 2019; Sterley et al., 2018). Both female and male mice spent
307 more time sniffing the anogenital and head/torso region of the stranger mice when compared with
308 the familiar conspecifics, with males spending a greater time engaged in anogenital sniffing
309 compared to females (Anogenital sniffing: two-way ANOVA; effect of conspecific: F(1, 26) = 18,

310 **p = 0.002, effect of sex: F(1, 26) = 8.19, **p = 0.0082; Head/torso sniffing: two-way ANOVA;
311 effect of conspecific: F(1, 26) = 3.17, p = 0.087, effect of sex: F(1, 26) = 0.99, p = 0.33) (**Figure
312 S6A, B**). The analysis of the hcrt activity peaks time locked to each behavior yielded a significantly
313 larger signal in female and male mice while they were engaged in the anogenital and head/torso
314 sniffing of the stranger mice, compared to sniffing the familiar conspecifics (Anogenital sniffing:
315 two-way ANOVA; effect of conspecific: F(1, 26) = 6.16, *p = 0.02, effect of sex: F(1, 26) = 3.62, p
316 = 0.068; Head/torso sniffing: two-way ANOVA; effect of conspecific: F(1, 26) = 7.21, *p = 0.012,
317 effect of sex: F(1, 26) = 2.6, p = 0.12) (**Figure S6C-S6F**). These data showed a stronger
318 anogenital sniffing drive and a borderline increase in the activity of the hcrt neuron population
319 during anogenital sniffing in male mice compared to females.

320 Taken together, our data showed that the activity of the LH hcrt neuron population
321 increases in response to social or object investigation. However, while the larger hcrt neuron
322 activity in response to novel social interaction indicates social discrimination, this difference in
323 activity is absent when mice interact with familiar or novel objects. The sex differences with males
324 responding to social interaction with larger anogenital sniffing and greater hcrt Ca^{2+} response
325 compared with females are also absent when mice are interacting with objects.

326 **Inhibition of hcrt neuron activity disrupts social behavior in male mice.** Having established
327 that the activity of hcrt neuron population is highly responsive to social interaction, we next
328 investigated whether hcrt neurons are required for social behavior. We infused a Cre-dependent
329 adeno-associated virus (AAV) encoding EYFP (controls) or the blue light-activated chloride
330 channel (iC++) (Berndt et al., 2016) into the LH of *Hcrt*$^{IRES\text{-}Cre}$ mice (**Figure 4A, B**). We validated
331 that hcrt neurons expressing iC++ are inhibited in response to blue light stimulation using *ex vivo*
332 electrophysiological recordings (**Figure S7A, B**). Because the first social interaction yields the
333 maximum signal, which correlates with the subsequent interaction amount, we employed a
334 photoinhibition protocol by silencing hcrt neurons in resident mice prior to the introduction of
335 familiar or stranger conspecifics into the home cage (**Figure 4C**). The social interaction test was

336 repeated on two separate days and the order of the conspecific was counterbalanced across
337 different days. Social interaction was quantified as the summation of anogenital and head/torso
338 sniffing. In female mice, the optogenetic inhibition of hcrt activity did not affect the time spent
339 interacting with familiar or stranger conspecifics (two-way ANOVA; effect of group: $F(1, 28) =$
340 1.64, $p = 0.21$, effect of conspecific: $F(1, 28) = 3.41$, $p = 0.07$) (**Figure 4D**). In contrast, male mice
341 spent significantly less time interacting with conspecifics when hcrt activity was inhibited (two-way
342 ANOVA; effect of group: $F(1, 24) = 13.82$, $p = 0.001$, effect of conspecific: $F(1, 24) = 2.66$, $p =$
343 0.12; Fisher's LSD; EYFP vs iC++: familiar, $p = 0.07$, stranger, $p = 0.002$) (**Figure 4E**). To verify
344 that the optogenetic activation of iC++ induces inhibition of hcrt neurons effectively, we perfused
345 a group of EYFP- and iC++-expressing mice 90 min after social interaction with a stranger
346 conspecific. cFos immunostaining revealed a significant reduction in cFos+ hcrt neurons in female
347 and male mice (two-way ANOVA; effect of group: $F(1, 11) = 12.62$, $p = 0.004$) (**Figure S7C, D**).
348 We further found that male mice showed an overall greater hcrt cFos expression compared to
349 females (two-way ANOVA; effect of sex: $F(1, 11) = 6.78$, $p = 0.02$) (**Figure S7C, D**).

350 To determine whether sociability is affected similarly in a more controlled setting in which
351 the stranger mouse is confined, we tested mice in a 3-chamber test while inhibiting hcrt neuron
352 activity. While we detected no difference for sociability in females (two-way ANOVA; effect of
353 group: $F(1, 28) = 2.59$, $p = 0.12$, effect of zone: $F(1, 28) = 26.56$, $p < 0.001$) (**Figure 4F, G**) and
354 control males (**Figure 4F, H**), all showing a greater preference for the confined stranger, male
355 iC++ mice spent comparable time in the social and non-social sniffing zones (two-way ANOVA;
356 group X zone interaction: $F(1, 22) = 4.81$, $p = 0.039$; Tukey's multiple comparisons test: EYFP
357 social vs non-social $p = 0.029$, iC++ social vs non-social $p = 0.99$) (**Figure 4H**).

358 Because hcrt neuron activity is linked to locomotion (Karnani et al., 2020) and can be
359 regulated by stress (Grafe et al., 2018, 2017; Sargin, 2019), we next investigated whether
360 inhibition of hcrt neurons affects locomotor or anxiety-like behavior. We performed open field and
361 elevated plus maze tests in the presence of blue light in EYFP- and iC++ expressing female and

362 male mice. Acute inhibition of hcrt neuron activity during open field test did not lead to changes
363 in distance traveled (two-way ANOVA; effect of group: $F(1, 25) = 1.46$, $p = 0.24$), or the time spent
364 in the outer or the inner zone of the open field apparatus (two-way ANOVA; effect of group for
365 time in outer zone: $F(1, 25) = 1.45$, $p = 0.24$, effect of group for time in inner zone: $F(1, 25) = 1.45$,
366 $p = 0.24$) in iC++ female and male mice, compared with mice expressing EYFP (**Figure S8A-D**).
367 In the open field test, both groups of female mice traveled a greater distance than male mice,
368 indicating greater locomotor activity in females regardless of group (two-way ANOVA; effect of
369 sex: $F(1, 25) = 4.62$, $^*p = 0.042$). Female mice also spent more time in the outer zone (two-way
370 ANOVA; effect of sex: $F(1, 25) = 4.64$, $^*p = 0.041$) and less time in the inner zone of the open
371 field (two-way ANOVA; effect of sex: $F(1, 25) = 4.64$, $^*p = 0.041$), compared with male mice
372 (**Figure S8A-D**). In the elevated plus maze, we did not detect a difference in locomotion (two-way
373 ANOVA; effect of group: $F(1, 23) = 0.64$, $p = 0.43$, effect of sex: $F(1, 23) = 3.02$, $p = 0.09$) or
374 anxiety-like behavior between the groups (two-way ANOVA; effect of group for time in closed
375 arms: $F(1, 23) = 1.21$, $p = 0.28$, effect of group for time in open arms: $F(1, 23) = 1.19$, $p = 0.28$)
376 or sexes (two-way ANOVA; effect of sex for time in closed arms: $F(1, 23) = 1.07$, $p = 0.31$, effect
377 of sex for time in open arms: $F(1, 23) = 0.67$, $p = 0.42$) (**Figure S8E-H**).

378 Overall, acute optogenetic inhibition of hcrt neuron activity significantly reduced the time
379 resident male mice spent interacting with the conspecifics, and decreased the preference of male
380 mice for the social conspecific without affecting locomotor activity or anxiety-like behavior. In
381 females, acute inhibition of hcrt neuron activity did not affect social interaction. These data
382 suggest that hcrt neurons are necessary for normative social behavior in male mice while in
383 females, the potential recruitment of different neural circuits may overcome the effects of reduced
384 hcrt activity on social interaction.

385 **Reduced hcrt-1 receptor signaling alters the activity of the insular cortex and VTA and**
386 **disrupts social interaction in male mice.** Hcrt neurons are a group of heterogeneous cells that
387 project to and modulate many different brain regions where they release hcrt and co-transmitters

388 including dynorphin (Chou et al., 2001; Li and van den Pol, 2006) or glutamate (Schöne et al.,
389 2012). To determine whether disrupted social interaction is dependent on hypocretin, we injected
390 male and female mice with the hcrt-1 receptor antagonist SB-334867 or vehicle 30 min before
391 social behavior (**Figure 5A**). Similar to the results of the optogenetic experiments, reduced hcrt-
392 1 receptor signaling with SB-334867 administration significantly decreased social interaction in
393 male mice only. SB-334867 did not lead to changes in the duration of time female mice engaged
394 with the stranger conspecifics compared with the vehicle treatment however, females interacted
395 with the stranger mice significantly less compared with male mice (two-way ANOVA; drug X sex
396 interaction: $F(1, 20) = 30.29$, $^{**}p < 0.001$, Tukey's multiple comparisons test: female vs male,
397 vehicle $^{**}p < 0.001$, female vs male SB-334867 $p = 0.53$; female vehicle vs female SB-334867, p
398 $= 0.36$, male vehicle vs male SB-334867, $^{**}p < 0.001$) (**Figure 5B**). To investigate the potential
399 effects of SB-334867 on the locomotor activity or anxiety-like behavior, we performed open field
400 right after vehicle and SB-334867 administrations and social behavior experiments (**Figure 5A**).
401 The total distance traveled in the open field were not different between vehicle- and SB-334867-
402 treated mice, with females traveling an overall greater distance compared to males (two-way
403 ANOVA, distance traveled; effect of drug: $F(1, 20) = 2.19$, $p = 0.15$, effect of sex: $F(1, 20) = 9.4$,
404 $^{**}p = 0.006$) (**Figure 5C**). Moreover, SB-334867 administration did not yield any significant
405 differences in the amount of time spent in the outer and inner zones of the open field (two-way
406 ANOVA, time in outer zone; effect of drug: $F(1, 20) = 2.1$, $p = 0.16$, effect of sex: $F(1, 20) = 1.7$, p
407 $= 0.21$, time in inner zone; effect of drug: $F(1, 20) = 2.1$, $p = 0.16$, effect of sex: $F(1, 20) = 1.69$, p
408 $= 0.21$) (**Figure 5D, E)**. This suggested that changes in locomotor activity or anxiety levels did not
409 contribute to the observed differences in social behavior.

410 We next investigated how social interaction in the presence or absence of hcrt-1 receptor
411 blockade affects the activity of cortical and subcortical regions that are modulated by hcrt inputs
412 and are implicated in social behavior. We perfused vehicle- and SB-334867-administered female
413 and male mice 90 min after social interaction with a stranger conspecific and then immunolabeled

414 the brains for cFos. We used the Flexible Atlas Segmentation Tool for Multi-Area Processing
415 (FASTMAP) machine-learning pipeline (Terstege et al., 2022) for high-throughput quantification
416 of cFos density in the insular, prelimbic, infralimbic cortical regions as well as the CA1 region of
417 the hippocampus, lateral amygdala (LA), the bed nucleus of the stria terminalis (BNST), nucleus
418 accumbens (NAc) and the ventral tegmental area (VTA). The comparison of the differences in
419 cFos density between SB-334867-admnistered female and male mice revealed significant
420 differences in two of the brain regions investigated. The density of cFos immunoreactive cells was
421 significantly increased by SB-334867 treatment relative to control mice in the insular cortex and
422 significantly decreased in the VTA of male mice, compared with females (two-way ANOVA; brain
423 region X sex interaction: $F(7, 80) = 4.12$, $p = 0.0007$, Bonferroni's multiple comparison; males vs
424 females, insular cortex $^{*}p = 0.02$, VTA $^{**}p = 0.005$) (**Figure 5G, H**). Similarly, compared to the
425 vehicle-injected mice, SB-334867-administered males showed significantly increased activity in
426 the insular cortex and decreased activity in the VTA (two-way ANOVA; brain region X drug
427 interaction: $F(7, 80) = 3.18$, $p = 0.005$, Bonferroni's multiple comparison test; vehicle vs SB-
428 334867, insular cortex $^{*}p = 0.016$, VTA $^{**}p = 0.026$) (**Figure S9A**). These changes were not
429 observed in females (two-way ANOVA; effect of drug: $F(1, 80) = 0.39$, $p = 0.53$, effect of brain
430 region: $F(7, 80) = 0.94$, $p = 0.48$) (**Figure S9B**). These data provide insights into the potential
431 circuits that hcrt modulates differentially in females and males during social interaction.
432

433 **Discussion**

434 Discrete neural subpopulations in the hypothalamus play a critical role in producing and
435 modulating a variety of social behaviors, such as mating, aggression, and social bonding
436 (Hashikawa et al., 2016; K. Hashikawa et al., 2017; Y. Hashikawa et al., 2017; Hull and
437 Dominguez, 2007; Scott et al., 2015; Wu et al., 2014; Yoshihara et al., 2018). Similarly, research
438 into the functional roles of hcrt neurons has begun to suggest that these cells are involved in the
439 neural substrates of social processes, but the nature and extent of their involvement has not yet

440 been determined. Here, using a combination of fiber photometry, optogenetic and
441 pharmacological inhibition and social interaction assays, we characterized the role of hcrt neuron
442 activity in social behavior. We demonstrate for the first time that the activity of hcrt neuron
443 population is regulated by social approach and interaction and is critical for social behavior in a
444 sex-dependent manner.

445 Photometry recordings revealed that hcrt neurons in female and male mice exhibit a robust
446 increase in activity in response to social interaction. The elevation in activity was prominent during
447 indirect social contact in the 3-chamber social interaction test or during reciprocal social
448 interaction in the familiar home cage or less familiar novel cage. Moreover, hcrt neuron activity
449 was more pronounced during interaction between unfamiliar mice compared to the increased
450 activity observed during familiar interactions. These experiments provide the first evidence that
451 the discrimination between familiar and unfamiliar conspecifics is differentially encoded by the
452 hcrt neuron activity. In contrast, the increase in hcrt neuron activity remained the same when mice
453 interacted with familiar or novel objects, suggesting that a greater population of hcrt neurons is
454 being recruited in response to social novelty.

455 Earlier work has implicated that hcrt signaling plays a role in social behavior. Accordingly,
456 male *Hcrt receptor 1* gene (*Hcrtr1*$^{-/-}$) null mutant mice exhibit reduced sociability and decreased
457 preference for social novelty compared to wild type mice (Abbas et al., 2015). Male orexin null
458 mutant mice show diminished behavioral response to an intruder in a resident-intruder paradigm
459 (Kayaba et al., 2003). A microdialysis study in human epileptic patients found maximal hcrt
460 release during social interactions (Blouin et al., 2013). While orexin/ataxin-3- transgenic mice with
461 hcrt cell loss show deficits in social memory (Yang et al., 2013). Supported by these studies, our
462 data suggest a novel role for hcrt neuron activity states in the encoding of social discrimination.
463 We also report a significant correlation between initial social approach and interaction-induced
464 hcrt neuron activity and the subsequent time mice spent engaging with stranger conspecifics,

465 suggesting that the initial approach-induced engagement of the hcrt neurons determines the
466 duration of subsequent social interaction.

467 While both females and males show greater hcrt activity in response to social interaction,
468 we obtained sex differences in the extent of hcrt activity and social interaction in females
469 compared with males. Overall, both the hcrt Ca^{2+} signal and amount of time spent in social sniffing
470 habituated faster in females throughout the reciprocal social interaction test. The faster
471 habituation of the hcrt neuron activity during social interaction in females may reflect a
472 disengagement of this system during the initial stages of interaction. A difference in sex-
473 dependent neural and social engagement is not surprising given the variable strategies utilized
474 by female and male mice in social behavior (Malloy et al., 2005; Okuyama et al., 2016; Rao et al.,
475 2019). Yet, while the optogenetic inhibition of hcrt neurons resulted in a deficit in the normal
476 behavior of male mice towards conspecifics, this did not lead to a change in sociability of females.
477 Pharmacological blockade of hcrt-1 receptors similarly disrupted social interaction in males only,
478 suggesting that sex-dependent hcrt neuron-induced modulation of social behavior is hcrt
479 dependent.

480 The difference in the activity phenotype of hcrt neurons may represent sex-specific
481 differences in local LH hcrt neuron network dynamics, which aligns with the sex differences
482 observed in other hypothalamic cell subpopulations (K. Hashikawa et al., 2017). The mechanisms
483 underlying the sex differences may also be in part be due to the differential stress response that
484 may be induced by same-sex social interactions in females and males. As social interactions may
485 be more rewarding to females than males (Borland et al., 2019), the extent of the engagement of
486 hcrt neurons in same-sex social interaction may be dependent on the positive or negative valence
487 to a social stimulus. In contrast, same-sex social interaction may be more stressful for males due
488 to their increased tendency to show aggressive behaviors when interacting with other males
489 (Malloy et al., 2005). Interestingly, the hcrt/orx system is highly regulated by stress in a sex-
490 dependent manner (Grafe and Bhatnagar, 2020). Although mice were not exposed to stress prior

491 to social interaction in our experiments, the capability of females for social buffering acute stress
492 responses (Sterley et al., 2018; Taylor et al., 2000) may be a potential determinant in the
493 differential engagement of neural populations based on the valence of the behavioral task.
494 Interestingly, inhibition of the paraventricular CRH neurons (that are under the excitatory
495 regulation of the hcrt system) (Bonnavion et al., 2015), similarly decreases social interaction in
496 male mice (Sterley et al., 2018). Altogether, the sex-dependent recruitment of hcrt neurons in
497 social behavior may have important implications for disorders associated with social deficits and
498 that are more prevalent in men compared with women (Silber et al., 2002; Werling and
499 Geschwind, 2013).

500 Hcrt neurons are key regulators of sleep, wakefulness and arousal (Carter et al., 2012; de
501 Lecea, 2021; Inutsuka and Yamanaka, 2013; Sakurai, 2005; Tyree et al., 2018). Increased hcrt
502 activity reduces sleep to wake transitions (Adamantidis et al., 2007; Carter et al., 2009) while
503 reduced hcrt signaling or ablation of hcrt neurons has been associated with deficits in wakefulness
504 and narcolepsy, respectively (Hara et al., 2001; Peyron et al., 2000; Sasaki et al., 2011;
505 Tsunematsu et al., 2011). Decreased arousal and wakefulness may contribute to a reduced
506 interest for social interaction. However, we did not find a change in locomotor activity upon acute
507 hcrt neuron inhibition or pharmacological blockade of hcrt-1 receptors, suggesting that reduced
508 interaction with conspecifics is not simply due to sedation. Given the strong association of
509 narcolepsy and social impairments (Morse and Sanjeev, 2018; Quaedackers et al., 2019), a
510 correlation between potential changes in sleep/wakefulness parameters and social interaction
511 upon acute hcrt inhibition will provide more insight. Due to the involvement of hcrt in stress
512 response (Grafe et al., 2018, 2017; Sargin, 2019), manipulation of hcrt neuron activity may
513 interfere with generalized anxiety states. However, we did not observe changes in general
514 anxiety-like behavior with acute hypocretin inhibition or hcrt-1 receptor antagonism, suggesting
515 that the association between reduced hcrt activity and social interaction may not be attributed
516 solely to changes in anxiety levels.

517 Hcrt neurons are located exclusively in the hypothalamus. However, they are a
518 heterogenous group of cells with distinct neurochemical and electrophysiological characteristics
519 (Mickelsen et al., 2017; Sagi et al., 2021). A substantial number of hcrt neurons co-express other
520 neuropeptides and transmitters including dynorphin (Chou et al., 2001), and glutamate (Henny et
521 al., 2010; Mickelsen et al., 2019; Schöne et al., 2012). Our experiments involving the blockade of
522 hcrt-1 receptors revealed a disruption in social interaction, thereby strengthening the involvement
523 of hcrt release in mediating social behavior. Further research is necessary to comprehensively
524 understand how the additional peptides and transmitters co-released by hcrt neurons may
525 potentially regulate social behavior. Recent research identified the expression of sex-specific
526 genes, *Ddx3y* and *Xist* in distinct clusters of hcrt neurons, suggesting a role for sexual dimorphism
527 in these neurons (Mickelsen et al., 2019). The specific role of these genes in hcrt-mediated sex
528 differences and the extent to which these hcrt clusters contribute to social interaction remain to
529 be determined. Furthermore, the bulk of our understanding of hcrt signaling has been derived
530 from studies primarily focused on males. In our experiments, we did not consider the estrous cycle
531 due to potential stress-related effects of the procedure as well as our experimental plan to include
532 a randomized group of females. The comparison of variances using Levene's test in key
533 experiments did not show a significant difference between females and males, which indicates
534 that sex-dependent differences in social interaction cannot be solely attributed to variations in
535 estrous cycles. The absence of androgen and estrogen receptors in hcrt neurons adds another
536 layer of complexity to the understanding of hcrt-mediated sex differences (Muschamp et al.,
537 2007). Furthermore, it is noteworthy that ovariectomy has been found to have no discernible effect
538 on the social interaction of females (Choi et al., 2022). This finding reinforces the importance of
539 exploring sex-dependent mechanisms that underlie social behavior from alternative perspectives,
540 allowing for a more comprehensive understanding.

541 To further investigate the mechanisms underlying the reduced hcrt signaling-induced
542 disruption in social behavior of male mice, we performed cFos-dependent activity mapping in

543 postsynaptic target regions that are targeted by hcrt neurons and are critical for social behavior.
544 We identified that the activity of two key brain regions, the insular cortex and the VTA were
545 significantly altered in male mice treated with the hcrt-1 receptor antagonist SB-334867 prior to
546 social interaction. In contrast, cFos levels were comparable between vehicle- and SB-334867
547 administered female mice. These findings show that, unlike in males, reduced hcrt signaling in
548 female mice does not result in alterations in social interaction or impact the social interaction
549 induced activity of the examined brain regions. The insular cortex plays a pivotal role in governing
550 emotional and interoceptive information (Gogolla, 2017; Wang et al., 2019), and is a vital
551 component of the network responsible for social decision-making and social affect (Rogers-Carter
552 et al., 2018). The VTA is also critical for motivated behavior, social reward and social approach
553 (Gunaydin et al., 2014). Both the insular cortex and VTA receive strong hcrt inputs and express
554 hcrt-1 receptors that modulate the activity of a variety of cell types in these regions (Hollander et
555 al., 2008; Thomas et al., 2022). The differential sex-dependent changes in the activity of these
556 regions point to potential circuits that are preferentially involved in hcrt-mediated social interaction.
557 Both the insular cortex and VTA show disrupted connectivity in patients with autism spectrum
558 disorders (ASD) and this is thought to be a contributing factor to the social impairments observed
559 in these conditions (Caria and de Falco, 2015; Ebisch et al., 2011; Huang et al., 2021; Uddin and
560 Menon, 2009). Given the higher prevalence of ASD in males, it is crucial to conduct further
561 research on the sex-dependent modulatory role of hcrt connections to these regions during social
562 behavior.

563 Overall, our findings provide a thorough characterization of hcrt neuron activity in social
564 interaction and situate the hcrt system as a critical part of a larger network that plays an integral
565 role in the modulation of social behavior. The observed sex differences further emphasize the
566 need for the incorporation of sex as a biological variable in the design of studies focusing on the
567 modulation of social behavior to understand the underlying mechanisms and circuits. Insights into

568 the role of the hcrt system in social behavior will particularly be important in paving the way for
569 novel treatment strategies targeting neuropsychiatric disorders associated with social deficits.
570

571 **Materials and Methods**

572 **Animals**

573 We used female and male mice (10 to 16-week old) *Hcrt*$^{IRES\text{-}Cre}$ mice on a C57BL6/J
574 background. Age-, and sex-matched C57BL6/J mice were used as strangers. For vehicle or SB-
575 334867 injections, C56Bl6/J mice were used. Mice were housed in standard housing conditions
576 on 12 h light/dark cycle (light on at 07:00) with water and food available *ad libitum*. All experiments
577 were conducted at the same time each day (12:00 – 16:00 pm). All experimental procedures were
578 performed in accordance with the guidelines established by the Canadian Council on Animal Care
579 and were approved by the Life and Environmental Sciences Animal Care Committee at the
580 University of Calgary.

581 **Generation of the *Hcrt*$^{IRES\text{-}Cre}$ knock-in mouse line**

582 *Hcrt*$^{IRES\text{-}Cre}$ mice were generated and gifted by Dr. Gina Leinninger. Briefly, a targeting
583 vector for homologous recombination was generated by inserting an internal ribosome entry site
584 (IRES)-Cre cassette into the 3' end of the *hypocretin* mRNA product. A frt-flanked neo cassette
585 was placed upstream of the IRES-Cre sequence. This *Hcrt*$^{IRES\text{-}Cre}$ targeting vector was linearized
586 and electroporated into C57/Bl6 mouse embryonic stem cells. DNA from ES cell clones was
587 analyzed via qPCR for loss of homozygosity using Taqman primer and probes for the genomic
588 *Hcrt* insertion sites (*Hcrt:* Forward: TTTACCAAGAGACTGACAGCG, Reverse:
589 CGGAGTCTGAACCCATCTTC, Probe: TCCTTGTCCTGATCCAAACTTCCCC). *NGF* was used
590 as a copy number control (Soliman et al., 2007). Putative positive ES clones were expanded,
591 confirmed for homologous recombination by Southern blot for neo and injected into blastocysts
592 to generate chimeric mice. Male chimeras were bred with C57BL/6 albino females and produced
593 germline progeny that express *Cre* and/or wild type *hcrt* (as assessed via PCR genotyping),

594 confirming successful establishment of the *Hcrt*$^{IRES\text{-}Cre}$ line. (Forward Cre: CAC TGA TTT CGA
595 CCA GGT TC, Reverse Cre: CAT CGC TCG ACC AGT TTA GT; Forward Hcrt wt: CTG GCT
596 GTG TGG AGT GAA A, Reverse Hcrt wt: GGG GGA AGT TTG GAT CAG G. Cre band = 255 bp,
597 Hcrt wt band = 460 bp).

598 *Hcrt*$^{IRES\text{-}Cre}$ mice were initially bred with *FlpO-Deleter* mice (Jackson Laboratories
599 *B6.129S4-Gt(ROSA)26Sor*$^{tm2(Flp^{*})Sor}$*/J*, stock #012930) to remove the frt-flanked neo cassette.
600 Neo-deleted *Hcrt*$^{IRES\text{-}Cre}$ mice were then bred with C57/BL/6J mice (Jackson Laboratory, Strain
601 #000664) to propagate the line.

602 **Stereotaxic Virus Injection and Optical Fiber Implantation**

603 Mice were anaesthetized with 5% isoflurane before being transferred to a stereotaxic head
604 frame (Kopf Instruments) and maintained at 2% isoflurane. Mice received analgesia (5 mg/kg
605 meloxicam, s.c.) and fluid support (Lactated Ringer's solution, s.c.) during surgery. Viral infusion
606 was performed using a glass micropipette attached to a Nanoject III infusion system (Drummond
607 Scientific) at 25 nl/sec for 10 sec. The infusion pipette was kept in place for 5 min after viral
608 delivery and slowly elevated over 5 min. The following coordinates were used for virus injections:
609 LH (from Bregma: AP -1.5 mm; ML ±1.0 mm; DV -5.2 mm). For fiber photometry experiments,
610 mice received a unilateral infusion of AAV9-CAG-flex-GcAMP6s.WIRE.SV40 (Addgene viral prep
611 # 100842-AAV9; 1.5 x 10^{13} vg/ml, 250 nl). For optogenetic experiments, mice received bilateral
612 infusions of AAV2/9-EF1a-DIO-iC++-EYFP (Canadian Neurophotonics Platform Viral Core
613 Facility RRID:SCR_016477; 1.7 x 10^{13} vg/ml, 250 nl per hemisphere) or AAV2/9-EF1a-DIO-EYFP
614 (Canadian Neurophotonics Platform Viral Core Facility RRID:SCR_016477; 1.9 x 10^{13} vg/ml, 250
615 nl per hemisphere).

616 For fiber photometry experiments, viral infusions were followed by implantation of mono
617 fiber optic cannulae (Neurophotometrics; 400 um, AP -1.5 mm; ML ±1.0 mm; DV -5.2 mm). For
618 optogenetic experiments, dual fiber optic cannulae (Doric Lenses; 200 um, AP -1.5 mm; ML ±1.0

619 mm; DV -4.9 mm) were used. Implants were secured to the skull using super glue and dental
620 cement. Behavior experiments were performed at least 3 weeks after surgery.

621 **Drug Injections**

622 The hcrt receptor-1 antagonist SB-334867 (HelloBio) was dissolved in sterile water
623 with 2% v/v DMSO and 10% w/v β-hydroxypropyl-cyclodextrin. SB-334867 or vehicle (2% v/v
624 DMSO and 10% w/v β-hydroxypropyl-cyclodextrin in water) was injected intraperitoneally at a
625 concentration of 30mg/kg 30 min prior to social interaction (Adamantidis et al., 2007; Ito et al.,
626 2008; Thomas et al., 2022).

627 ***In vivo* Fiber Photometry Recording and Analysis**

628 A Doric Lenses fiber photometry system with an LED driver and console was used to
629 deliver the 405 nm isosbestic control and 465 nm excitation light during recordings. LEDs were
630 connected to a Mini Cube filter set and a dichroic mirror array was used to permit simultaneous
631 delivery of excitation light through a low autofluorescence mono fiber-optic patch cord to the fiber
632 optic cannulae. The signal was detected by a photoreceiver (Newport Visible Femtowatt
633 Photoreceiver Module Model 2151). A lock-in amplification mode controlled by the Doric Studio
634 software was implemented (modulation frequencies: 208.6 Hz for 456 nm, 166.9 Hz for 405 nm,
635 cut-off frequency for demodulated signal: 12 Hz). Light power was calibrated to deliver 30 μW
636 light at the tip of the fiber using a photometer (Thor Labs).

637 The Doric Lenses fiber photometry console was set to trigger recording on remote delivery
638 of a time-to-live (TTL) pulse from a separate computer running ANY-maze behavior capture
639 software to time lock video and photometry recordings. Data from photometry and behavioral
640 recordings were extracted and exported to MATLAB (MathWorks). Using custom MATLAB
641 analyses, the 405 nm channel was used as an isosbestic control and the data recorded using this
642 channel was fit to a biexponential decay. Data from the Ca^{2+}-dependent 465 nm channel were
643 then linearly scaled using the fitted decay of the isosbestic channel, correcting for any
644 photobleaching which occurred during the recordings (Meng et al., 2018). The resulting vector

645 was converted to a ΔF/F trace as previously described (Evans et al., 2022), and each trace was
646 normalized as a z-score (Reichenbach et al., 2022). Z-scored ΔF/F traces were analyzed for area
647 under the curve, peak frequency, and maximum fluorescence.

648 For social behavior recordings in home and novel cages, mice were first habituated to the
649 fiber for 5 min. Fiber photometry analysis was conducted based on the baseline of 20 sec prior to
650 the initiation of the social behavior test. 20 sec baseline period was selected to avoid the effects
651 of the activity changes that can take place within a longer time window and may mask social
652 interaction-induced changes that take place minutes after. Area under the curve was
653 operationally defined as the summed area between the X-axis and the z-scored ΔF/F trace.
654 Comparisons of AUC during specific behaviors were normalized by the summed duration of the
655 behavioral epochs of interest. Peak frequency was refined using a peak detection filter of 2
656 standard deviations above the median z-scored ΔF/F value of the recording session (Evans et
657 al., 2022; Moda-Sava et al., 2019). For all behavior-specific analyses, photometry and behavioral
658 timeseries vectors were aligned using nearest-neighbours approximation to account for
659 differences in framerates across recording modalities.

660 ***In vivo* Optogenetic Inhibition**

661 Mice expressing EYFP (AAV2/9-EF1a-DIO-EYFP) or the inhibitory opsin iC++ (AAV2/9-
662 EF1a-DIO-iC++-EYFP) were used for optogenetic inhibition experiments. Laser driver (Opto
663 Engine LLC) was connected to a 1 x 2 fiber optic rotary joint (Doric Lenses) attached to a dual
664 fiber-optic patch cord. Mice were habituated to the patch cord for 5 min prior to starting the
665 behavior experiments. Blue light (470 nm, 17 mW) was delivered continuously via ANY-Maze
666 software-controlled AMi-2 optogenetic interface (Stoelting Co.) connected to the laser driver.

667 **Behavioral Testing**

668 The order of behavior tests was counterbalanced to control for any effect of testing order.
669 Before each test, the area around and under cages or the surfaces of the apparatus were sprayed

670 with 70% ethanol and wiped down with paper towel to reduce any residual odour. Prior to testing,
671 mice were handled and habituated to the fiber optic patch cord for 4 days.

672 ***3-Chamber Social Interaction Test***

673 The 3-chamber social interaction test was performed in two-stages in an acrylic 105 cm X
674 45 cm apparatus containing two plexiglass dividers, splitting the chamber into three equal areas.
675 During the habituation stage, each mouse was first placed in the middle chamber for 5 min. The
676 removal of the dividers allowed mice to freely explore the chamber for an additional 5 min. During
677 the test stage, one area contained a sex- and age-matched C57BL/6J mouse confined in an
678 inverted pencil cup (social zone) while the other area contained an empty cup (non-social zone).
679 Mice were first placed in the middle chamber with dividers in place for 5 min. Dividers were then
680 removed and mice were allowed to explore the chamber for 5 min. Time spent in each area was
681 tracked and analyzed using ANY-Maze video tracking software (Stoelting Co.).

682 ***Reciprocal Social Interaction Test***

683 To examine reciprocal social behavior, resident experimental mice were kept in their home cage.
684 Cage mates were separated for at least 15 min. For fiber photometry experiments, 5 min after
685 being connected to the fiber optic patch cord, the cage mate (familiar mouse) of the experimental
686 mouse was placed in the home cage and animals were allowed to freely interact for 5 min. 5 min
687 after removal of the cage mate, a sex- and age-matched C57BL/6J mouse (stranger mouse) was
688 placed in the home cage, and mice were allowed to freely interact for 5 min. For optogenetic
689 experiments, the tests were spread across two consecutive days to reduce the likelihood of
690 potential effects of prolonged light delivery and continual photoinhibition. The order of familiar or
691 stranger mice introduced into the home cage of the experimental mice was counterbalanced
692 across days. Blue light (470 nm, 17 mW) was turned on to allow 2 min of initial inhibition before
693 the introduction of the familiar or stranger mouse. The experimental mouse and conspecific were
694 allowed to freely interact for 5 min during continuous light delivery. Reciprocal social behavior in
695 a novel cage was examined using the similar paradigm above in a novel mouse cage with new

696 bedding material. Different stranger mice were introduced to mice tested in home cage and novel
697 cage experiments. Multiple social encounters have been avoided to keep stranger mice
698 unfamiliar. Different familiar mice were used in each day and cage mates were tested on different
699 days. All videos were recorded using ANY-Maze video tracking software (Stoelting Co.).

700 **Social Behavior Analysis**

701 We used the open-source automated positional tracking and behavioral classifications
702 algorithms DeepLabCut (DLC; (Lauer et al., 2021) and Simple Behavior Analysis (SimBA;
703 (Nilsson et al., 2020) to allow for unbiased, high-precision quantification and machine analysis of
704 social behavior. A subset of social interaction trials was also manually scored by an experimenter
705 blind to the groups to validate the resulting behavioral classifiers. Behavioral classifiers from
706 SimBA quantified social behavior as the time the experimental mice engage in head-torso sniffing
707 (snout of the experimental mouse was in direct proximity or direct contact with the head or torso
708 of a conspecific) and anogenital sniffing (snout of the experimental mouse was in direct proximity
709 to the anogenital region of a conspecific, including when actively following behind and sniffing a
710 conspecific). Social novelty index was calculated as follows: (% time interacting with stranger –
711 % time interacting with familiar) / (%time interacting with stranger + % time interacting with
712 familiar).

713 *Machine Scoring*

714 For automated analysis of social behavior using behavioral classification algorithms, video
715 recordings of social behavior experiments were first exported from ANY-maze to 20 frames-per-
716 second MP4 video files. A subset of these video files was imported into DLC, where the
717 experimenter blinded to the groups labelled the nose, left & right ears, left & right latissimus dorsi,
718 tail base, and the centre of the torso for each animal present in the frames. These frames were
719 then used by DLC to train the neural network to label the seven body parts described above. The
720 trained neural network then analyzed all video recordings of social behavior experiments to track
721 and plot the Cartesian coordinates of animals' body parts for every frame of each video. This

722 effectively provided the detailed spatial location of mice for every point in time throughout the
723 experiment.

724 The results of the positional tracking analysis from DLC were exported to SimBA. We used
725 a supervised-learning deep neural network within SimBA to create predictive classifiers for head-
726 torso and anogenital sniffing. The resulting predictive classifiers were then used to automatically
727 identify patterns in the positional data from DLC. Automated behavioral labels were validated for
728 accuracy by reviewing visualizations of classification results produced by SimBA.

729 For verification, all results from SimBA were visualized and reviewed by the experimenter,
730 and a subset of experiments were hand-scored to compare against the results of the automated
731 analysis. The results of SimBA's predictive classification for each experiment were exported for
732 both analysis of behavior alone and combined analysis with the photometry recordings from the
733 respective experiment. For photometry experiments, SimBA data and raw photometry traces were
734 imported and aligned by a custom MATLAB script. For optogenetic experiments, SimBA data
735 were analyzed and plotted.

736 ***Object Interaction Test***

737 Mice were made familiar with an object (a small plastic puzzle piece) placed in their home
738 cage for 72 h prior to the day of testing. A round glass marble was used as a novel object. 5 min
739 after being connected to the fiber optic patch cord, novel or familiar object was introduced into the
740 home cage of the experimental mouse. Each mouse was allowed to interact with the objects for
741 5 min. Videos were tracked and the time spent with each object was analyzed using ANY-Maze
742 software (Stoelting Co.).

743 ***Open Field Test***

744 Mice were placed in an acrylic 40 cm x 40 cm apparatus and allowed to explore for 5 min.
745 Blue light (470 nm, 17 mW) was kept on continuously while the animal was in the open field.
746 Videos were recorded and the total distance traveled, and the time spent in the outer and inner
747 zones were analyzed using ANY-Maze video tracking software (Stoelting Co.).

748 ***Elevated Plus Maze***

749 Mice were placed in the center of a plus-shaped apparatus consisting of two closed (36
750 cm) and two open (36 cm) arms. Blue light (470 nm, 17 mW) was kept on continuously while mice
751 were allowed to explore for 5 min. Videos were recorded and the total distance traveled, and the
752 time spent in each arm were analyzed using ANY-Maze video tracking software (Stoelting Co.).

753 **Slice Electrophysiology**

754 400 µm coronal slices comprising the LH were obtained in ice-cold oxygenated sucrose-
755 substituted artificial cerebrospinal fluid (ACSF) using a Leica VT1000 S vibratome. Slices were
756 recovered in aCSF (128 mM NaCl, 10 mM D-glucose, 26 mM $NaHCO_3$, 2 mM $CaCl_2$, 2 mM
757 $MgSO_4$, 3 mM KCl, 1.25 mM NaH_2PO_4, pH 7.4) for a minimum of 2 hours. During recovery and
758 recordings, slices were saturated with 95% O_2/5% CO_2 at 30°C. Recording was performed in
759 oxygenated aCSF flowing at a rate of 3-4 ml/min. The internal patch solution contained 120 mM
760 potassium gluconate, 10 mM HEPES, 5 mM KCl, 2 mM $MgCl_2$, 4 mM K_2-ATP, 0.4 mM Na_2-GTP,
761 10 mM Na_2-phosphocreatine, with pH adjusted to 7.3. Neurons were visualized using IR-DIC on
762 an Olympus BX51WI microscope and hcrt neurons were identified based on the expression of
763 EYFP. Whole-cell recordings were obtained in current clamp mode using a MultiClamp 700B
764 amplifier (Molecular Devices). Optogenetic inhibition through activation of iC++ was elicited using
765 CoolLED pE-300^{ultra} illumination system at 470 nm. Data were filtered at 4 kHz and digitized at 20
766 kHz using Digidata 1550B and Clampex software (Molecular Devices).

767 **Histology, Immunohistochemistry and Imaging**

768 Mice were then deeply anaesthetized by isoflurane and transcardially perfused with 0.1 M
769 PBS and 4% paraformaldehyde (PFA). Brains were extracted and post-fixed in 4 % PFA for 24 h
770 and cryoprotected in 30% sucrose in 0.1 M PBS for 3-5 days until sunk. Brains were frozen and
771 40 µM thick coronal sections were obtained using a cryo-microtome (ThermoFisher) and collected
772 in 6 series. Sections were stored in an antifreeze solution containing 30 % ethylene glycol, and
773 20 % glycerol in 0.1 M PBS and stored at -20°C for further analysis.

774 For immunolabeling, sections were washed three times in 0.1 M PBS for 10 min each.
775 Sections were incubated with goat anti-hypocretin-1/orexin A antibody (1:500, Santa Cruz, sc-
776 8070) and/or rabbit anti-melanin concentrating hormone (MCH) (1:500, Phoenix
777 Pharmaceuticals), rabbit anti-GFP (1:500, Invitrogen) or with rabbit anti-cFos (1:1000, SYSY)
778 antibodies diluted in 3 % normal donkey serum, 0.3 % Triton-X and 0.1 M PBS for 24 h. After
779 three washes with 0.1 M PBS for 10 min each, sections were incubated with donkey anti-goat
780 Alexa Fluor 594 (1:500, Jackson ImmunoResearch) and/or anti-goat Alexa Fluor 647 (1:500,
781 Invitrogen), or anti-rabbit Alexa Fluor 647 (1:500, Invitrogen) diluted in 0.1 M PBS for 24 h. After
782 three 10 min washes with 0.1 M PBS, sections were mounted on glass slides and coverslipped
783 with PVA-DABCO mounting medium. Sections immunostained for cFos were were incubated with
784 DAPI (1:500, HelloBio) in PBS for 15 min and washed three times in 0.1 M PBS before mounting.
785 Sections were imaged using an Olympus FV3000 confocal microscope. Images were
786 acquired with a 10X and 60X oil immersion objectives, with the aperture set to 1 airy unit. Z-stack
787 image sequences were maximum intensity projected as a 2D image using Fiji. 2-3 sections
788 comprising the LH were analyzed per mouse. Quantification of cells labeled with GFP and
789 hypocretin-1 was performed using Fiji image processing software. Only mice with accurate
790 stereotaxic targeting and viral expression were included in the analyses. For cFos analysis,
791 sections were scanned at 10X magnification using a slide scanner (OLYMPUS VS120-L100-W;
792 Richmond Hill, ON, CA). cFos positive cells were segmented from background based on
793 fluorescent intensity and label morphology using *Ilastik* (Berg et al., 2019). Images were then
794 registered to the Allen Brain Institute mouse brain reference atlas to assess the expression
795 density of segmented cFos positive cells using FASTMAP (Terstege et al., 2022). Cells in the
796 following regions were quantified: Insular cortex, infralimbic cortex, prelimbic cortex, CA1 region
797 of the hippocampus, lateral amygdala, bed nucleus of the stria terminalis (BNST), nucleus
798 accumbens (NAc), and the ventral tegmental area (VTA). The expression density was calculated
799 as the number of cFos positive cells divided by the area of the region for each brain section.

800 **Statistical Analysis**

801 Statistical analysis was performed using GraphPad Prism 9, except three-way ANOVAs which
802 were conducted using Statistica software. Tukey's multiple comparisons tests were applied when
803 the F test for the interaction is significant (Rosner, 2000). In the absence of a significant
804 interaction, we planned a priori comparisons between the groups and separately analyzed these
805 comparisons using Fisher's LSD test. These differences are indicated on the graphs with an
806 octothorpe signal. In cFos mapping experiments, Bonferroni adjustments were used to reduce
807 the risk of Type 1 error with the large number of regions analyzed. The AUC of the Ca2+ signal
808 from one mouse in Figure 1 was identified to be an outlier (Grubb's test; alpha = 0.05, G= 1.77,
809 outlier Y = 533.7) and removed from the analysis. All statistical data are reported in
810 Supplementary Tables S1-S5.

811 **Acknowledgements**

812 We thank the transgenic cores at University of Michigan and Van Andel Research Institute for
813 assistance generating *Hcrt*$^{IRES\text{-}Cre}$ mice. David P. Olson graciously shared the Cre-inducible
814 Rosa$^{eGFP\text{-}L10a}$ reporter line used in these studies. Funding for this study was provided by an
815 NSERC Discovery Grant (RGPIN-2020-05305) and an Arrell Family Foundation Future Leader in
816 Canadian Brain Research grant to DS, an NSERC Discovery Grant (RGPIN-2018-05135) to JRE.
817 DJT received fellowships from NSERC and the Canadian Open Neuroscience Platform. DP
818 received Harley Hotchkiss-Samuel Weiss Postdoctoral Fellowship.

819 **Author contributions**

820 D.S. and M.D. designed the experiments and wrote the manuscript. R.B. and G.M.L. designed
821 and made the mouse line. N.J. and M.T. performed the surgeries. M.D. and D.P. performed the
822 behavioral experiments. M.D. performed the histological procedures. D.S., M.D., D.J.T. and
823 J.R.E. conducted the analysis.

824 **Data availability**

All data that support the findings of this study are present in the manuscript and the supplementary materials, and are available from the corresponding author upon request.

Code availability

All custom scripts used for photometry analysis are publicly available in a GitHub repository (https://github.com/dterstege/PublicationRepo/tree/main/Dawson2022).

Declaration of Interests

The authors declare no competing interests.

Figure Legends

Figure 1. Increase in hcrt neuron activity in response to social investigation. A) Schematic (left) and a representative image (right) showing viral targeting and expression of GCaMP6s in LH hcrt neurons. **B)** Hypocretin-1 (blue) and GCaMP6s (red) co-localization in the LH of a *Hcrt*$^{IRES\text{-}Cre}$ mouse infused with the AAV-CAG-Flex-GCaMP6s. Scale bar, 20 um. **C)** 3-chamber social interaction paradigm during fiber photometry. Social and non-social zones are the compartments of the chamber that harbor the social target or the empty cup, respectively. Sniffing zones are defined as the area around the perimeter of the holder zones. **D)** Averaged hcrt Ca^{2+} traces over time aligned to the time of entrance (t = 0 sec) into the social zone in female mice (n = 4 mice). **E)** The hcrt Ca^{2+} signal for each mouse showing baseline (-1 to 0 sec), entrance (0 sec) and peak response after the entrance into the social zone (0-2 sec). In female mice, the hcrt Ca^{2+} signal increased upon entrance into the social and non-social zones and the activity in each zone was comparable (two-way ANOVA; effect of time: $F(2, 18) = 15.96$, $p < 0.001$, effect of zone: $F(1, 18) = 0.07$, $p = 0.79$). **F)** In female mice, the area under the curve of the averaged hcrt Ca^{2+} responses after entrance into social and non-social zones did not differ (paired t-test; $p = 0.96$). **G)** Averaged hcrt Ca^{2+} traces over time aligned to the time of entrance (t = 0 sec) into the social zone in male mice (n = 5 mice). **H)** In male mice, the hcrt Ca^{2+} signal increased upon entrance into the social and non-social zones and the activity in social zone was significantly greater than activity in the

non-social zone (two-way ANOVA; effect of time: F(2, 24) = 12.86, p = 0.0002, effect of zone: F(1,24) = 11.2, **p = 0.0027). **I)** In male mice, the area under the curve of the averaged hcrt Ca^{2+} responses after entrance into the social zone was significantly greater compared to the non-social zone (paired t-test; *p = 0.025). **J)** A representative hcrt Ca^{2+} photometry trace aligned to the time spent in social (red) and non-social (black) sniffing zones from a female (above) and a male mouse (below). **K)** The maximum hcrt Ca^{2+} signal during interaction with the social target was larger compared with that during non-social target interaction regardless of sex (two-way ANOVA; effect of zone: F(1, 14) = 6.55, *p = 0.023, effect of sex: F(1, 14) = 4.56, p = 0.051). This difference was significant only in males (Fisher's LSD; social vs non-social: females, p = 0.69, males, $^{\#\#}p$ = 0.004). **L)** The frequency of activity (peaks/sec) during interaction with the social target was significantly larger compared to the non-social interaction. In females, the frequency of hcrt activity was larger during social and non-social interactions, compared with the male mice (two-way ANOVA; effect of zone: F(1, 14) = 7.77, p = 0.014, effect of sex: F(1, 14) = 9.15, **p = 0.009). Planned comparisons revealed a significant difference for males but not females (Fisher's LSD; social vs non-social: females, p = 0.16, males, $^{\#}p$ = 0.024). **M)** The area under the curve of the hcrt Ca^{2+} signal in each sniffing zone, normalized by the duration of time spent in each zone was significantly larger during interaction with the social target compared with the non-social target in male mice only (two-way ANOVA; zone X sex interaction: F(1, 14) = 6.74, p = 0.021; Tukey's multiple comparisons test: Social vs non-social sniffing zone; Males **p = 0.006, females p = 0.99). Data represent mean ± SEM. The complete statistical output is shown in Supplementary Table S1.

Figure 2. Differential hcrt neuron activity during social interaction in home cage. A) Experimental paradigm showing social interaction test during fiber photometry. After baseline recordings for 5 min in the home cage, the resident experimental mouse is introduced to a familiar (cage mate) followed by a stranger (novel) mouse. **B)** Heatmaps showing hcrt Ca^{2+} signal for each mouse 20 sec prior to and 2 min after being introduced to a familiar (top) or a stranger

877 (bottom) mouse. Data are aligned to initial approach by the resident mouse. **C)** Averaged Ca^{2+}
878 signal changes in hcrt neurons in female (n = 7) and male (n = 8) mice during interaction with a
879 stranger or a familiar mouse. The hcrt neuron activity peaks right after initial approach initiated by
880 the experimental mouse and returns to baseline within 2 min. **D)** Representative hcrt Ca^{2+} traces
881 from an experimental mouse during interaction with a stranger or a familiar mouse. **E)** The area
882 under the curve of the hcrt Ca^{2+} response within the first 2 min of social behavior is larger when
883 the resident mice interact with a stranger compared with a familiar mouse (two-way ANOVA; effect
884 of conspecific: $F(1, 26) = 8.96$, $^{**}p = 0.006$, effect of sex: $F(1, 26) = 1.78$, $p = 0.19$; Fisher's LSD;
885 familiar vs stranger: females, $p = 0.1$, males, $^{\#}p = 0.016$). **F)** The maximum hcrt Ca^{2+} signal in
886 response to initial approach and sniffing is larger when the resident mice are introduced to a
887 stranger compared to a familiar cage mate. The hcrt Ca^{2+} signal is larger in male mice compared
888 to female mice during interaction with familiar and stranger conspecifics (two-way ANOVA; effect
889 of conspecific: $F(1, 26) = 8.01$, $^{**}p = 0.009$, effect of sex: $F(1, 26) = 8.29$, $^{**}p = 0.008$; Fisher's
890 LSD; familiar vs stranger: females, $^{\#}p = 0.03$, males, $p = 0.09$). **G)** Scatter plot showing the
891 correlation between the maximum hcrt Ca^{2+} signal in the resident mice and the time they spent
892 sniffing the stranger ($r(13)=0.58$, $^{*}p=0.023$) or the familiar ($r(13)=0.37$, $p=0.18$) conspecific. **(H)**
893 The maximum hcrt Ca^{2+} signal in the resident mice over time during social behavior is shown for
894 both females and males. The greater hcrt activity right after first approach and sniffing decreased
895 over time in both females and males (three-way ANOVA; time X conspecific interaction: $F(14,$
896 $364) = 2.32$, $p = 0.004$; Tukey's multiple comparisons test: Stranger vs familiar at 20 sec $^{*}p =$
897 0.035, 40 sec $^{**}p = 0.009$, all other time points $p's > 0.05$). Male mice showed a greater hcrt Ca^{2+}
898 signal within the first minute of social behavior, compared with females (three-way ANOVA; time
899 X sex interaction: $F(14, 364) = 2.19$, $p = 0.007$; Tukey's multiple comparisons test: Male vs female
900 at 20 sec $^{\#}p = 0.013$, 40 sec $^{\#}p = 0.033$, all other time points $p's > 0.05$). **I)** Time spent sniffing by
901 the resident mice over time during social behavior is shown for females and males. Mice spent
902 more time sniffing the stranger compared to familiar, which declined over time (three-way ANOVA;

903 time X conspecific interaction: F (14, 364) = 3.46, $p < 0.001$, Tukey's multiple comparisons test:
904 Stranger vs familiar at 40 sec $^{**}p < 0.001$, 60 sec $^{**}p = 0.0013$, 80 sec $^{**}p = 0.005$ all other time
905 points *p's* > 0.05). Male mice engaged more in social interaction than females (three-way ANOVA;
906 effect of sex: F(1, 26) = 4.62, $p = 0.041$). Data represent mean ± SEM. The complete statistical
907 output is shown in Supplementary Table S2.

908 **Figure 3. Differential hcrt activity during social interaction persists in a non-territorial**
909 **setting and is absent during object investigation. A)** Experimental paradigm showing social
910 interaction in the novel cage test during fiber photometry. After baseline recordings for 5 min in a
911 cage with novel bedding, the resident experimental mouse is introduced to a familiar (cage mate)
912 followed by a stranger (novel) mouse. **B)** Heatmaps showing hcrt Ca^{2+} signal for each mouse 20
913 sec prior to and 2 min after being introduced to a familiar (top) or a stranger (bottom) mouse. Data
914 are aligned to initial approach by the experimental mouse. **C)** Averaged Ca^{2+} signal changes in
915 hcrt neurons in female (n = 5) and male (n = 6) mice during interaction with a stranger or a familiar
916 mouse in the novel cage. The hcrt neuron activity peaks right after initial approach initiated by the
917 experimental mouse and returns to baseline within 2 min. **D)** The area under the curve of the hcrt
918 Ca^{2+} response within the first 2 min of social behavior is larger when the experimental mice interact
919 with a stranger compared with a familiar mouse (two-way ANOVA; effect of conspecific: F(1, 18)
920 = 4.91, $^{*}p = 0.038$, effect of sex: F(1, 18) = 2.83, $p = 0.11$). **E)** The maximum hcrt Ca^{2+} signal in
921 response to initial approach and sniffing is larger when the experimental mice are introduced to a
922 stranger compared to a familiar cage mate. The hcrt Ca^{2+} signal is greater in male mice compared
923 to female mice regardless of the social interaction type (two-way ANOVA; effect of conspecific:
924 F(1, 18) = 19.14, $^{**}p = 0.0004$, effect of sex: F(1, 18) = 4.87, $^{*}p = 0.041$; Fisher's LSD; familiar vs
925 stranger: females, $^{\#\#}p = 0.006$, males, $^{\#\#}p = 0.006$). **F)** Scatter plot showing the correlation
926 between the maximum hcrt Ca^{2+} signal in the experimental mice and the time they spent sniffing
927 the stranger r(13)=0.69, $^{*}p$=0.018) or the familiar (r(13)=0.46, p=0.16) conspecific. **G)**
928 Experimental paradigm showing fiber photometry during object interaction test. After baseline

929 recordings for 5 min in the home cage, the resident experimental mouse is introduced to a familiar
930 or a novel object. **H)** Averaged Ca^{2+} signal changes in hcrt neurons in female (n = 7) and male (n
931 = 8) mice during interaction with a familiar or a novel object in the home cage, aligned to the time
932 of initial approach to the object. **I)** The area under the curve of the hcrt Ca^{2+} response within the
933 first 2 min of object interaction is comparable when the experimental mice interact with novel or
934 familiar objects (two-way ANOVA; effect of object: $F(1, 26) = 1.97$, $p = 0.17$, effect of sex: $F(1, 26)$
935 $= 0.21$, $p = 0.65$). **J)** The maximum hcrt Ca^{2+} signal in response to initial approach to familiar and
936 novel objects is comparable (two-way ANOVA; effect of object: $F(1, 26) = 0.013$, $p = 0.91$, effect
937 of sex: $F(1, 26) = 0.35$, $p = 0.56$). *$p<0.05$, **$p<0.01$, ns; non-significant. Data represent mean ±
938 SEM. The complete statistical output is shown in Supplementary Table S3.

939 **Figure 4. Acute optogenetic inhibition of hcrt neuron activity disrupts social interaction in**
940 **male mice. A)** Schematic (left) and a representative image showing viral targeting and expression
941 of iC++ in LH hcrt neurons. **B)** Hypocretin-1 (red) and iC++ (cyan) co-localization in the LH of a
942 *Hcrt*$^{IRES\text{-}Cre}$ mouse infused with the AAV-EF1a-DIO-iC++-EYFP. Scale bar, 100 um. **C)**
943 Experimental paradigm showing 5 min social interaction with familiar or stranger mice after 5 min
944 of fiber habituation and 2 min of hcrt neuron inhibition. Blue light was kept on during social
945 interaction. Each interaction was performed on different days and the order of conspecific was
946 counterbalanced. **D)** In female mice, optogenetic inhibition of hcrt neuron activity did not affect
947 the time spent interacting with familiar or stranger conspecifics (two-way ANOVA; effect of group:
948 $F(1, 28) = 1.64$, $p = 0.21$, effect of conspecific: $F(1, 28) = 3.41$, $p = 0.07$). **E)** Inhibition of hcrt
949 neuron activity in male mice reduced interaction time with conspecifics, compared with EYFP
950 mice (two-way ANOVA; effect of group: $F(1, 24) = 13.82$, **$p = 0.001$, effect of conspecific: $F(1,$
951 $24) = 2.66$, $p = 0.12$; Fisher's LSD; EYFP vs iC++: familiar, $p = 0.07$, stranger, $^{\#\#}p = 0.002$). **F)**
952 Representative tracks from female and male EYFP and iC++ mice during in 3-chamber sociability
953 task in the presence of blue light. **G)** Inhibition of hcrt neuron activity did not lead to a change in
954 sociability in females in 3-chamber test (two-way ANOVA; effect of group: $F(1, 28) = 2.59$, $p =$

955 0.12, effect of zone: F(1, 28) = 26.56, $p < 0.001$). **H)** Male iC++ mice spent comparable time in
956 the social and non-social sniffing zones of the 3-chamber in contrast to male EYFP mice (two-
957 way ANOVA; group X zone interaction: F(1, 22) = 4.81, *p = 0.039; Tukey's multiple comparisons
958 test: EYFP social vs non-social p = 0.029, iC++ social vs non-social p = 0.99). Data represent
959 mean ± SEM. The complete statistical output is shown in Supplementary Table S4.

960 **Figure 5. Blocking hcrt-1 receptors with SB334867 disrupts social interaction in male mice**
961 **and is accompanied by alterations in the activity of the insular cortex and VTA. A)**
962 Experimental paradigm. Mice were first injected with either 30mg/kg of SB-334867 or vehicle. 30
963 min after injection, mice interacted with a novel conspecific for 5 min, followed by 5 min exploration
964 in the open field. **B)** Injection of SB-334867 reduced social interaction with stranger conspecifics
965 in male mice, without an effect in females (two-way ANOVA; drug X sex interaction: F (1, 20) =
966 30.29, **$p < 0.001$, Tukey's multiple comparisons test: Females vs males, vehicle **$p < 0.001$,
967 SB-334867 p = 0.53; Females vehicle vs SB-334867, p = 0.36, males vehicle vs SB-334867, **p
968 < 0.001). **C)** Total distance traveled is comparable between vehicle- and SB-334867-injected
969 mice. Females traveled significantly greater distance in the open field, compared with males (two-
970 way ANOVA; effect of drug: F(1, 20) = 2.19, p = 0.15, effect of sex: F(1, 20) = 9.4, **p = 0.006).
971 The time spent in the outer zone **(D)** and the inner zone **(E)** of the open field is comparable
972 between mice. **F)** Experimental paradigm. 30 min after vehicle or SB-334867 injection, mice were
973 allowed to interact with a stranger conspecific for 5 min. Mice were perfused 90 min after social
974 interaction. Brains were processed for cFos immunohistochemistry. **G)** Male mice injected with
975 SB-334867 had significantly greater cFos density in the insular cortex and reduced cFos density
976 in the VTA, compared with females injected with SB-334867 (two-way ANOVA; brain region X
977 sex interaction: F(7, 80) = 4.12, p = 0.0007, Bonferroni's multiple comparison test; males vs
978 females, insular cortex *p = 0.02, VTA **p = 0.005). **H**) Representative images showing DAPI
979 (blue) and cFos (red) immunostaining in the insular cortex and VTA of female and male mice.

980 **References**

Abbas MG, Shoji H, Soya S, Hondo M, Miyakawa T, Sakurai T. 2015. Comprehensive Behavioral Analysis of Male Ox1r−/− Mice Showed Implication of Orexin Receptor-1 in Mood, Anxiety, and Social Behavior. *Front Behav Neurosci* **9**. doi:10.3389/fnbeh.2015.00324

Adamantidis AR, Zhang F, Aravanis AM, Deisseroth K, de Lecea L. 2007. Neural substrates of awakening probed with optogenetic control of hypocretin neurons. *Nature* **450**:420–424. doi:10.1038/nature06310

Anderson DJ. 2016. Circuit modules linking internal states and social behaviour in flies and mice. *Nat Rev Neurosci* **17**:692–704. doi:10.1038/nrn.2016.125

Berg S, Kutra D, Kroeger T, Straehle CN, Kausler BX, Haubold C, Schiegg M, Ales J, Beier T, Rudy M, Eren K, Cervantes JI, Xu B, Beuttenmueller F, Wolny A, Zhang C, Koethe U, Hamprecht FA, Kreshuk A. 2019. Ilastik: Interactive machine learning for (bio)image analysis. *Nat Methods* **16**:1226–1232. doi:10.1038/s41592-019-0582-9

Berndt A, Lee SY, Wietek J, Ramakrishnan C, Steinberg EE, Rashid AJ, Kim H, Park S, Santoro A, Frankland PW, Iyer SM, Pak S, Ährlund-Richter S, Delp SL, Malenka RC, Josselyn SA, Carlén M, Hegemann P, Deisseroth K. 2016. Structural foundations of optogenetics: Determinants of channelrhodopsin ion selectivity. *Proc Natl Acad Sci U S A* **113**:822–829. doi:10.1073/pnas.1523341113

Bisetti A, Cvetkovic V, Serafin M, Bayer L, Machard D, Jones BE, Mühlethaler M. 2006. Excitatory action of hypocretin/orexin on neurons of the central medial amygdala. *Neuroscience* **142**:999–1004. doi:10.1016/j.neuroscience.2006.07.018

Blouin AM, Fried I, Wilson CL, Staba RJ, Behnke EJ, Lam HA, Maidment NT, Karlsson KÆ, Lapierre JL, Siegel JM. 2013. Human hypocretin and melanin-concentrating hormone levels are linked to emotion and social interaction. *Nat Commun* **4**:1547. doi:10.1038/ncomms2461

Bonnavion P, Jackson AC, Carter ME, de Lecea L. 2015. Antagonistic interplay between hypocretin and leptin in the lateral hypothalamus regulates stress responses. *Nat Commun* **6**:6266. doi:10.1038/ncomms7266

Borland JM, Aiani LM, Norvelle A, Grantham KN, O'Laughlin K, Terranova JI, Frantz KJ, Albers HE. 2019. Sex-dependent regulation of social reward by oxytocin receptors in the ventral tegmental area. *Neuropsychopharmacology* **44**:785–792. doi:10.1038/s41386-018-0262-y

Bourgin P, Huitrón-Résendiz S, Spier AD, Fabre V, Morte B, Criado JR, Sutcliffe JG, Henriksen SJ, de Lecea L. 2000. Hypocretin-1 modulates rapid eye movement sleep through activation of locus coeruleus neurons. *J Neurosci* **20**:7760–7765. doi:10.1523/JNEUROSCI.20-20-07760.2000

Caria A, de Falco S. 2015. Anterior insular cortex regulation in autism spectrum disorders. *Front Behav Neurosci* **9**:38. doi:10.3389/fnbeh.2015.00038

Carter ME, Adamantidis A, Ohtsu H, Deisseroth K, de Lecea L. 2009. Sleep homeostasis modulates hypocretin-mediated sleep-to-wake transitions. *J Neurosci* **29**:10939–10949. doi:10.1523/JNEUROSCI.1205-09.2009

Carter ME, Brill J, Bonnavion P, Huguenard JR, Huerta R, de Lecea L. 2012. Mechanism for Hypocretin-mediated sleep-to-wake transitions. *Proc Natl Acad Sci U S A* **109**:E2635-44. doi:10.1073/pnas.1202526109

Chen P, Hong W. 2018. Neural Circuit Mechanisms of Social Behavior. *Neuron* **98**:16–30. doi:10.1016/j.neuron.2018.02.026

Choi JE, Choi DI, Lee J, Kim J, Kim MJ, Hong I, Jung H, Sung Y, Kim J-I, Kim T, Yu N-K, Lee S-H, Choe HK, Koo JW, Kim J-H, Kaang B-K. 2022. Synaptic ensembles between raphe and D1R-containing accumbens shell neurons underlie postisolation sociability in males. *Sci Adv* **8**:eabo7527. doi:10.1126/sciadv.abo7527

1030 Chou TC, Lee CE, Lu J, Elmquist JK, Hara J, Willie JT, Beuckmann CT, Chemelli RM, Sakurai T,
1031 Yanagisawa M, Saper CB, Scammell TE. 2001. Orexin (hypocretin) neurons contain
1032 dynorphin. *J Neurosci* **21**:RC168. doi:10.1523/jneurosci.21-19-j0003.2001
1033 Clancy AN, Coquelin A, Macrides F, Gorski RA, Noble EP. 1984. Sexual behavior and aggression
1034 in male mice: involvement of the vomeronasal system. *J Neurosci* **4**:2222–2229.
1035 doi:10.1523/JNEUROSCI.04-09-02222.1984
1036 de Lecea L. 2021. Twenty-Three Years of Hypocretins: The 'Rosetta Stone' of Sleep/Arousal
1037 Circuits. *Front Neurol Neurosci* **45**:1–10. doi:10.1159/000514961
1038 de Lecea L, Kilduff TS, Peyron C, Gao X, Foye PE, Danielson PE, Fukuhara C, Battenberg EL,
1039 Gautvik VT, Bartlett FS 2nd, Frankel WN, van den Pol AN, Bloom FE, Gautvik KM, Sutcliffe
1040 JG. 1998. The hypocretins: hypothalamus-specific peptides with neuroexcitatory activity.
1041 *Proc Natl Acad Sci U S A* **95**:322–327. doi:10.1073/pnas.95.1.322
1042 Del Cid-Pellitero E, Garzón M. 2011. Hypocretin1/OrexinA-containing axons innervate locus
1043 coeruleus neurons that project to the Rat medial prefrontal cortex. Implication in the sleep-
1044 wakefulness cycle and cortical activation. *Synapse* **65**:843–857. doi:10.1002/syn.20912
1045 Ebisch SJH, Gallese V, Willems RM, Mantini D, Groen WB, Romani GL, Buitelaar JK, Bekkering
1046 H. 2011. Altered intrinsic functional connectivity of anterior and posterior insula regions in
1047 high-functioning participants with autism spectrum disorder. *Hum Brain Mapp* **32**:1013–
1048 1028. doi:10.1002/hbm.21085
1049 España RA, Melchior JR, Roberts DCS, Jones SR. 2011. Hypocretin 1/orexin A in the ventral
1050 tegmental area enhances dopamine responses to cocaine and promotes cocaine self-
1051 administration. *Psychopharmacology* **214**:415–426. doi:10.1007/s00213-010-2048-8
1052 España RA, Oleson EB, Locke JL, Brookshire BR, Roberts DCS, Jones SR. 2010. The
1053 hypocretin-orexin system regulates cocaine self-administration via actions on the
1054 mesolimbic dopamine system. *Eur J Neurosci* **31**:336–348. doi:10.1111/j.1460-
1055 9568.2009.07065.x
1056 Evans A, Terstege DJ, Scott GA, Tsutsui M, Epp JR. 2022. Neurogenesis mediated plasticity is
1057 associated with reduced neuronal activity in CA1 during context fear memory retrieval. *Sci*
1058 *Rep* **12**:7016. doi:10.1038/s41598-022-10947-w
1059 Fadel J, Burk JA. 2010. Orexin/hypocretin modulation of the basal forebrain cholinergic system:
1060 Role in attention. *Brain Res* **1314**:112–123. doi:10.1016/j.brainres.2009.08.046
1061 Fadel J, Deutch AY. 2002. Anatomical substrates of orexin-dopamine interactions: lateral
1062 hypothalamic projections to the ventral tegmental area. *Neuroscience* **111**:379–387.
1063 doi:10.1016/s0306-4522(02)00017-9
1064 Fadel J, Frederick-Duus D. 2008. Orexin/hypocretin modulation of the basal forebrain cholinergic
1065 system: insights from in vivo microdialysis studies. *Pharmacol Biochem Behav* **90**:156–
1066 162. doi:10.1016/j.pbb.2008.01.008
1067 Giardino WJ, Eban-Rothschild A, Christoffel DJ, Li S-B, Malenka RC, de Lecea L. 2018. Parallel
1068 circuits from the bed nuclei of stria terminalis to the lateral hypothalamus drive opposing
1069 emotional states. *Nat Neurosci* **21**:1084–1095. doi:10.1038/s41593-018-0198-x
1070 Gogolla N. 2017. The insular cortex. *Curr Biol* **27**:R580–R586. doi:10.1016/j.cub.2017.05.010
1071 Grafe LA, Bhatnagar S. 2020. The contribution of orexins to sex differences in the stress
1072 response. *Brain Res* **1731**:145893. doi:10.1016/j.brainres.2018.07.026
1073 Grafe LA, Cornfeld A, Luz S, Valentino R, Bhatnagar S. 2017. Orexins Mediate Sex Differences
1074 in the Stress Response and in Cognitive Flexibility. *Biol Psychiatry* **81**:683–692.
1075 doi:10.1016/j.biopsych.2016.10.013
1076 Grafe LA, Eacret D, Dobkin J, Bhatnagar S. 2018. Reduced Orexin System Function Contributes
1077 to Resilience to Repeated Social Stress. *eNeuro* **5**. doi:10.1523/ENEURO.0273-17.2018
1078 Gunaydin LA, Grosenick L, Finkelstein JC, Kauvar IV, Fenno LE, Adhikari A, Lammel S,
1079 Mirzabekov JJ, Airan RD, Zalocusky KA, Tye KM, Anikeeva P, Malenka RC, Deisseroth

K. 2014. Natural neural projection dynamics underlying social behavior. *Cell* **157**:1535–1551. doi:10.1016/j.cell.2014.05.017

Hara J, Beuckmann CT, Nambu T, Willie JT, Chemelli RM, Sinton CM, Sugiyama F, Yagami K, Goto K, Yanagisawa M, Sakurai T. 2001. Genetic ablation of orexin neurons in mice results in narcolepsy, hypophagia, and obesity. *Neuron* **30**:345–354. doi:10.1016/s0896-6273(01)00293-8

Hasegawa E, Maejima T, Yoshida T, Masseck OA, Herlitze S, Yoshioka M, Sakurai T, Mieda M. 2017. Serotonin neurons in the dorsal raphe mediate the anticataplectic action of orexin neurons by reducing amygdala activity. *Proc Natl Acad Sci U S A* **114**:E3526–E3535. doi:10.1073/pnas.1614552114

Hasegawa E, Yanagisawa M, Sakurai T, Mieda M. 2014. Orexin neurons suppress narcolepsy via 2 distinct efferent pathways. *J Clin Invest* **124**:604–616. doi:10.1172/JCI71017

Hashikawa K, Hashikawa Y, Falkner A, Lin D. 2016. The neural circuits of mating and fighting in male mice. *Curr Opin Neurobiol* **38**:27–37. doi:10.1016/j.conb.2016.01.006

Hashikawa K, Hashikawa Y, Tremblay R, Zhang J, Feng JE, Sabol A, Piper WT, Lee H, Rudy B, Lin D. 2017. Esr1+ cells in the ventromedial hypothalamus control female aggression. *Nat Neurosci* **20**:1580–1590. doi:10.1038/nn.4644

Hashikawa Y, Hashikawa K, Falkner AL, Lin D. 2017. Ventromedial Hypothalamus and the Generation of Aggression. *Front Syst Neurosci* **11**:94. doi:10.3389/fnsys.2017.00094

Henny P, Brischoux F, Mainville L, Stroh T, Jones BE. 2010. Immunohistochemical evidence for synaptic release of glutamate from orexin terminals in the locus coeruleus. *Neuroscience* **169**:1150–1157. doi:10.1016/j.neuroscience.2010.06.003

Hofer MA. 1996. Multiple regulators of ultrasonic vocalization in the infant rat. *Psychoneuroendocrinology* **21**:203–217. doi:10.1016/0306-4530(95)00042-9

Hollander JA, Lu Q, Cameron MD, Kamenecka TM, Kenny PJ. 2008. Insular hypocretin transmission regulates nicotine reward. *Proc Natl Acad Sci U S A* **105**:19480–19485. doi:10.1073/pnas.0808023105

Hong W, Kim D-W, Anderson DJ. 2014. Antagonistic control of social versus repetitive self-grooming behaviors by separable amygdala neuronal subsets. *Cell* **158**:1348–1361. doi:10.1016/j.cell.2014.07.049

Huang Y, Yu S, Wilson G, Park J, Cheng M, Kong X, Lu T, Kong J. 2021. Altered extended locus coeruleus and ventral tegmental area networks in boys with autism spectrum disorders: A resting-state functional connectivity study. *Neuropsychiatr Dis Treat* **17**:1207–1216. doi:10.2147/NDT.S301106

Hull EM, Dominguez JM. 2007. Sexual behavior in male rodents. *Horm Behav* **52**:45–55. doi:10.1016/j.yhbeh.2007.03.030

Inutsuka A, Yamanaka A. 2013. The regulation of sleep and wakefulness by the hypothalamic neuropeptide orexin/hypocretin. *Nagoya J Med Sci* **75**:29–36.

Ito N, Yabe T, Gamo Y, Nagai T, Oikawa T, Yamada H, Hanawa T. 2008. I.c.v. administration of orexin-A induces an antidepressive-like effect through hippocampal cell proliferation. *Neuroscience* **157**:720–732. doi:10.1016/j.neuroscience.2008.09.042

Karnani MM, Schöne C, Bracey EF, González JA, Viskaitis P, Li H-T, Adamantidis A, Burdakov D. 2020. Role of spontaneous and sensory orexin network dynamics in rapid locomotion initiation. *Prog Neurobiol* **187**:101771. doi:10.1016/j.pneurobio.2020.101771

Kayaba Y, Nakamura A, Kasuya Y, Ohuchi T, Yanagisawa M, Komuro I, Fukuda Y, Kuwaki T. 2003. Attenuated defense response and low basal blood pressure in orexin knockout mice. *Am J Physiol Regul Integr Comp Physiol* **285**:R581-93. doi:10.1152/ajpregu.00671.2002

Keller M, Douhard Q, Baum MJ, Bakker J. 2006. Sexual experience does not compensate for the disruptive effects of zinc sulfate--lesioning of the main olfactory epithelium on sexual behavior in male mice. *Chem Senses* **31**:753–762. doi:10.1093/chemse/bjl018

1131 Kingsbury L, Huang S, Wang J, Gu K, Golshani P, Wu YE, Hong W. 2019. Correlated Neural
1132 Activity and Encoding of Behavior across Brains of Socially Interacting Animals. *Cell*
1133 **178**:429-446.e16. doi:10.1016/j.cell.2019.05.022
1134 Lauer J, Zhou M, Ye S, Menegas W, Nath T, Rahman MM, Di Santo V, Soberanes D, Feng G,
1135 Murthy VN, Lauder G, Dulac C, Mathis MW, Mathis A. 2021. Multi-animal pose estimation
1136 and tracking with DeepLabCut. *bioRxiv*. doi:10.1101/2021.04.30.442096
1137 Lee W, Fu J, Bouwman N, Farago P, Curley JP. 2019. Temporal microstructure of dyadic social
1138 behavior during relationship formation in mice. *PLoS One* **14**:e0220596.
1139 doi:10.1371/journal.pone.0220596
1140 Li Y, van den Pol AN. 2006. Differential target-dependent actions of coexpressed inhibitory
1141 dynorphin and excitatory hypocretin/orexin neuropeptides. *J Neurosci* **26**:13037–13047.
1142 doi:10.1523/JNEUROSCI.3380-06.2006
1143 Li Y, Zhong W, Wang D, Feng Q, Liu Z, Zhou J, Jia C, Hu F, Zeng J, Guo Q, Fu L, Luo M. 2016.
1144 Serotonin neurons in the dorsal raphe nucleus encode reward signals. *Nat Commun* **7**.
1145 doi:10.1038/ncomms10503
1146 Lo L, Yao S, Kim D-W, Cetin A, Harris J, Zeng H, Anderson DJ, Weissbourd B. 2019.
1147 Connectional architecture of a mouse hypothalamic circuit node controlling social
1148 behavior. *Proc Natl Acad Sci U S A* **116**:7503–7512. doi:10.1073/pnas.1817503116
1149 Lungwitz EA, Molosh A, Johnson PL, Harvey BP, Dirks RC, Dietrich A, Minick P, Shekhar A, Truitt
1150 WA. 2012. Orexin-A induces anxiety-like behavior through interactions with glutamatergic
1151 receptors in the bed nucleus of the stria terminalis of rats. *Physiol Behav* **107**:726–732.
1152 doi:10.1016/j.physbeh.2012.05.019
1153 Malloy TE, Barcelos S, Arruda E, DeRosa M, Fonseca C. 2005. Individual differences and cross-
1154 situational consistency of dyadic social behavior. *J Pers Soc Psychol* **89**:643–654.
1155 doi:10.1037/0022-3514.89.4.643
1156 Marlin BJ, Mitre M, D'amour JA, Chao MV, Froemke RC. 2015. Oxytocin enables maternal
1157 behaviour by balancing cortical inhibition. doi:10.1038/nature14402
1158 Meng C, Zhou J, Papaneri A, Peddada T, Xu K, Cui G. 2018. Spectrally Resolved Fiber
1159 Photometry for Multi-component Analysis of Brain Circuits. *Neuron* **98**:707-717.e4.
1160 doi:10.1016/j.neuron.2018.04.012
1161 Mickelsen LE, Bolisetty M, Chimileski BR, Fujita A, Beltrami EJ, Costanzo JT, Naparstek JR,
1162 Robson P, Jackson AC. 2019. Single-cell transcriptomic analysis of the lateral
1163 hypothalamic area reveals molecularly distinct populations of inhibitory and excitatory
1164 neurons. *Nat Neurosci* **22**:642–656. doi:10.1038/s41593-019-0349-8
1165 Mickelsen LE, Kolling FW 4th, Chimileski BR, Fujita A, Norris C, Chen K, Nelson CE, Jackson
1166 AC. 2017. Neurochemical Heterogeneity Among Lateral Hypothalamic Hypocretin/Orexin
1167 and Melanin-Concentrating Hormone Neurons Identified Through Single-Cell Gene
1168 Expression Analysis. *eNeuro* **4**. doi:10.1523/ENEURO.0013-17.2017
1169 Mitchell CS, Fisher SD, Yeoh JW, Pearl AJ, Burton NJ, Bains JS, McNally GP, Andrews ZA,
1170 Graham BA, Dayas CV. 2020. A ventral striatal-orexin/hypocretin circuit modulates
1171 approach but not consumption of food. *bioRxiv*. doi:10.1101/2020.03.05.979468
1172 Moda-Sava RN, Murdock MH, Parekh PK, Fetcho RN, Huang BS, Huynh TN, Witztum J, Shaver
1173 DC, Rosenthal DL, Alway EJ, Lopez K, Meng Y, Nellissen L, Grosenick L, Milner TA,
1174 Deisseroth K, Bito H, Kasai H, Liston C. 2019. Sustained rescue of prefrontal circuit
1175 dysfunction by antidepressant-induced spine formation. *Science* **364**.
1176 doi:10.1126/science.aat8078
1177 Morse AM, Sanjeev K. 2018. Narcolepsy and Psychiatric Disorders: Comorbidities or Shared
1178 Pathophysiology? *Med Sci (Basel)* **6**. doi:10.3390/medsci6010016
1179 Moy SS, Nadler JJ, Perez A, Barbaro RP, Johns JM, Magnuson TR, Piven J, Crawley JN. 2004.
1180 Sociability and preference for social novelty in five inbred strains: an approach to assess

autistic-like behavior in mice. *Genes Brain Behav* **3**:287–302. doi:10.1111/j.1601-1848.2004.00076.x

Muschamp JW, Dominguez JM, Sato SM, Shen R-Y, Hull EM. 2007. A role for hypocretin (orexin) in male sexual behavior. *J Neurosci* **27**:2837–2845. doi:10.1523/JNEUROSCI.4121-06.2007

Nilsson SRO, Goodwin NL, Choong JJ, Hwang S, Wright HR, Norville ZC, Tong X, Lin D, Bentzley BS, Eshel N, McLaughlin RJ, Golden SA. 2020. Simple Behavioral Analysis (SimBA) – an open source toolkit for computer classification of complex social behaviors in experimental animals. *bioRxiv*. doi:10.1101/2020.04.19.049452

Okuyama T. 2018. Social memory engram in the hippocampus. *Neurosci Res* **129**:17–23. doi:10.1016/j.neures.2017.05.007

Okuyama T, Kitamura T, Roy DS, Itohara S, Tonegawa S. 2016. Ventral CA1 neurons store social memory. *Science* **353**:1536–1541. doi:10.1126/science.aaf7003

Payet JM, Wilson K-E, Russo AM, Angiolino A, Kavanagh-Ryan W, Kent S, Lowry CA, Hale MW. 2021. Involvement of dorsal raphe nucleus serotonergic systems in social approach-avoidance behaviour and in the response to fluoxetine treatment in peri-adolescent female BALB/c mice. *Behav Brain Res* **408**:113268. doi:10.1016/j.bbr.2021.113268

Peyron C, Faraco J, Rogers W, Ripley B, Overeem S, Charnay Y, Nevsimalova S, Aldrich M, Reynolds D, Albin R, Li R, Hungs M, Pedrazzoli M, Padigaru M, Kucherlapati M, Fan J, Maki R, Lammers GJ, Bouras C, Kucherlapati R, Nishino S, Mignot E. 2000. A mutation in a case of early onset narcolepsy and a generalized absence of hypocretin peptides in human narcoleptic brains. *Nat Med* **6**:991–997. doi:10.1038/79690

Quaedackers L, van Gilst MM, van Mierlo P, Lammers G-J, Dhondt K, Amesz P, Peeters E, Hendriks D, Vandenbussche N, Pillen S, Overeem S. 2019. Impaired social functioning in children with narcolepsy. *Sleep* **42**. doi:10.1093/sleep/zsy228

Rao RP, von Heimendahl M, Bahr V, Brecht M. 2019. Neuronal Responses to Conspecifics in the Ventral CA1. *Cell Rep* **27**:3460-3472.e3. doi:10.1016/j.celrep.2019.05.081

Reichenbach A, Clarke RE, Stark R, Lockie SH, Mequinion M, Dempsey H, Rawlinson S, Reed F, Sepehrizadeh T, DeVeer M, Munder AC, Nunez-Iglesias J, Spanswick DC, Mynatt R, Kravitz AV, Dayas CV, Brown R, Andrews ZB. 2022. Metabolic sensing in AgRP neurons integrates homeostatic state with dopamine signalling in the striatum. *Elife* **11**. doi:10.7554/eLife.72668

Rogers-Carter MM, Varela JA, Gribbons KB, Pierce AF, McGoey MT, Ritchey M, Christianson JP. 2018. Insular cortex mediates approach and avoidance responses to social affective stimuli. *Nat Neurosci* **21**:404–414. doi:10.1038/s41593-018-0071-y

Rosner BR. 2000. Fundamentals of Biostatistics, 5th ed. Florence, AL: Duxbury Press.

Sagi D, de Lecea L, Appelbaum L. 2021. Heterogeneity of hypocretin/orexin neurons. *Front Neurol Neurosci* **45**:61–74. doi:10.1159/000514964

Sakurai T. 2005. Roles of orexin/hypocretin in regulation of sleep/wakefulness and energy homeostasis. *Sleep Med Rev* **9**:231–241. doi:10.1016/j.smrv.2004.07.007

Sakurai T, Amemiya A, Ishii M, Matsuzaki I, Chemelli RM, Tanaka H, Williams SC, Richardson JA, Kozlowski GP, Wilson S, Arch JR, Buckingham RE, Haynes AC, Carr SA, Annan RS, McNulty DE, Liu WS, Terrett JA, Elshourbagy NA, Bergsma DJ, Yanagisawa M. 1998. Orexins and orexin receptors: a family of hypothalamic neuropeptides and G protein-coupled receptors that regulate feeding behavior. *Cell* **92**:573–585. doi:10.1016/s0092-8674(00)80949-6

Samson WK, Taylor MM, Follwell M, Ferguson AV. 2002. Orexin actions in hypothalamic paraventricular nucleus: physiological consequences and cellular correlates. *Regul Pept* **104**:97–103. doi:10.1016/s0167-0115(01)00353-6

Saper CB, Lowell BB. 2014. The hypothalamus. *Curr Biol* **24**:R1111-6. doi:10.1016/j.cub.2014.10.023

1232 Sargin D. 2019. The role of the orexin system in stress response. *Neuropharmacology* **154**:68–
1233 78. doi:10.1016/j.neuropharm.2018.09.034
1234 Sasaki K, Suzuki M, Mieda M, Tsujino N, Roth B, Sakurai T. 2011. Pharmacogenetic modulation
1235 of orexin neurons alters sleep/wakefulness states in mice. *PLoS One* **6**:e20360.
1236 doi:10.1371/journal.pone.0020360
1237 Schöne C, Cao ZFH, Apergis-Schoute J, Adamantidis A, Sakurai T, Burdakov D. 2012.
1238 Optogenetic probing of fast glutamatergic transmission from hypocretin/orexin to
1239 histamine neurons in situ. *J Neurosci* **32**:12437–12443. doi:10.1523/JNEUROSCI.0706-
1240 12.2012
1241 Scott N, Prigge M, Yizhar O, Kimchi T. 2015. A sexually dimorphic hypothalamic circuit controls
1242 maternal care and oxytocin secretion. *Nature* **525**:519–522. doi:10.1038/nature15378
1243 Silber MH, Krahn LE, Olson EJ, Pankratz VS. 2002. The epidemiology of narcolepsy in Olmsted
1244 County, Minnesota: a population-based study. *Sleep* **25**:197–202.
1245 doi:10.1093/sleep/25.2.197
1246 Soliman GA, Ishida-Takahashi R, Gong Y, Jones JC, Leshan RL, Saunders TL, Fingar DC, Myers
1247 MG Jr. 2007. A simple qPCR-based method to detect correct insertion of homologous
1248 targeting vectors in murine ES cells. *Transgenic Res* **16**:665–670. doi:10.1007/s11248-
1249 007-9110-2
1250 Sterley T-L, Baimoukhametova D, Füzesi T, Zurek AA, Daviu N, Rasiah NP, Rosenegger D, Bains
1251 JS. 2018. Social transmission and buffering of synaptic changes after stress. *Nat Neurosci*
1252 **21**:393–403. doi:10.1038/s41593-017-0044-6
1253 Takahashi A, Nagayasu K, Nishitani N, Kaneko S, Koide T. 2014. Control of intermale aggression
1254 by medial prefrontal cortex activation in the mouse. *PLoS One* **9**:e94657.
1255 doi:10.1371/journal.pone.0094657
1256 Taylor SE, Klein LC, Lewis BP, Gruenewald TL, Gurung RA, Updegraff JA. 2000. Biobehavioral
1257 responses to stress in females: tend-and-befriend, not fight-or-flight. *Psychol Rev*
1258 **107**:411–429. doi:10.1037/0033-295x.107.3.411
1259 Terstege DJ, Oboh DO, Epp JR. 2022. FASTMAP: Open-Source Flexible Atlas Segmentation
1260 Tool for Multi-Area Processing of Biological Images. *eNeuro* **9**.
1261 doi:10.1523/ENEURO.0325-21.2022
1262 Thomas CS, Mohammadkhani A, Rana M, Qiao M, Baimel C, Borgland SL. 2022. Optogenetic
1263 stimulation of lateral hypothalamic orexin/dynorphin inputs in the ventral tegmental area
1264 potentiates mesolimbic dopamine neurotransmission and promotes reward-seeking
1265 behaviours. *Neuropsychopharmacology* **47**:728–740. doi:10.1038/s41386-021-01196-y
1266 Tsunematsu T, Kilduff TS, Boyden ES, Takahashi S, Tominaga M, Yamanaka A. 2011. Acute
1267 optogenetic silencing of orexin/hypocretin neurons induces slow-wave sleep in mice. *J*
1268 *Neurosci* **31**:10529–10539. doi:10.1523/JNEUROSCI.0784-11.2011
1269 Tyree SM, Borniger JC, de Lecea L. 2018. Hypocretin as a Hub for Arousal and Motivation. *Front*
1270 *Neurol* **9**:413. doi:10.3389/fneur.2018.00413
1271 Uddin LQ, Menon V. 2009. The anterior insula in autism: under-connected and under-examined.
1272 *Neurosci Biobehav Rev* **33**:1198–1203. doi:10.1016/j.neubiorev.2009.06.002
1273 Unger EK, Burke KJ Jr, Yang CF, Bender KJ, Fuller PM, Shah NM. 2015. Medial amygdalar
1274 aromatase neurons regulate aggression in both sexes. *Cell Rep* **10**:453–462.
1275 doi:10.1016/j.celrep.2014.12.040
1276 van den Berg WE, Lamballais S, Kushner SA. 2015. Sex-specific mechanism of social hierarchy
1277 in mice. *Neuropsychopharmacology* **40**:1364–1372. doi:10.1038/npp.2014.319
1278 Veening JG, Coolen LM. 2014. Neural mechanisms of sexual behavior in the male rat: emphasis
1279 on ejaculation-related circuits. *Pharmacol Biochem Behav* **121**:170–183.
1280 doi:10.1016/j.pbb.2013.12.017

Vittoz NM, Schmeichel B, Berridge CW. 2008. Hypocretin /orexin preferentially activates caudomedial ventral tegmental area dopamine neurons. *Eur J Neurosci* **28**:1629–1640. doi:10.1111/j.1460-9568.2008.06453.x

Wang Q-P, Koyama Y, Guan J-L, Takahashi K, Kayama Y, Shioda S. 2005. The orexinergic synaptic innervation of serotonin- and orexin 1-receptor-containing neurons in the dorsal raphe nucleus. *Regul Pept* **126**:35–42. doi:10.1016/j.regpep.2004.08.030

Wang X, Wu Q, Egan L, Gu X, Liu P, Gu H, Yang Y, Luo J, Wu Y, Gao Z, Fan J. 2019. Anterior insular cortex plays a critical role in interoceptive attention. *Elife* **8**:e42265. doi:10.7554/eLife.42265

Wei D, Talwar V, Lin D. 2021. Neural circuits of social behaviors: Innate yet flexible. *Neuron* **109**:1600–1620. doi:10.1016/j.neuron.2021.02.012

Werling DM, Geschwind DH. 2013. Sex differences in autism spectrum disorders. *Curr Opin Neurol* **26**:146–153. doi:10.1097/WCO.0b013e32835ee548

Wu Z, Autry AE, Bergan JF, Watabe-Uchida M, Dulac CG. 2014. Galanin neurons in the medial preoptic area govern parental behaviour. *Nature* **509**:325–330. doi:10.1038/nature13307

Xie Y, Dorsky RI. 2017. Development of the hypothalamus: conservation, modification and innovation. *Development* **144**:1588–1599. doi:10.1242/dev.139055

Yang C, Zhang L, Hao H, Ran M, Li J, Dong H. 2019. Serotonergic neurons in the dorsal raphe nucleus mediate the arousal-promoting effect of orexin during isoflurane anesthesia in male rats. *Neuropeptides* **75**:25–33. doi:10.1016/j.npep.2019.03.004

Yang L, Zou B, Xiong X, Pascual C, Xie James, Malik A, Xie Julian, Sakurai T, Xie XS. 2013. Hypocretin/orexin neurons contribute to hippocampus-dependent social memory and synaptic plasticity in mice. *J Neurosci* **33**:5275–5284. doi:10.1523/JNEUROSCI.3200-12.2013

Yoshihara C, Numan M, Kuroda KO. 2018. Oxytocin and Parental Behaviors. *Curr Top Behav Neurosci* **35**:119–153. doi:10.1007/7854_2017_11

Figure 1

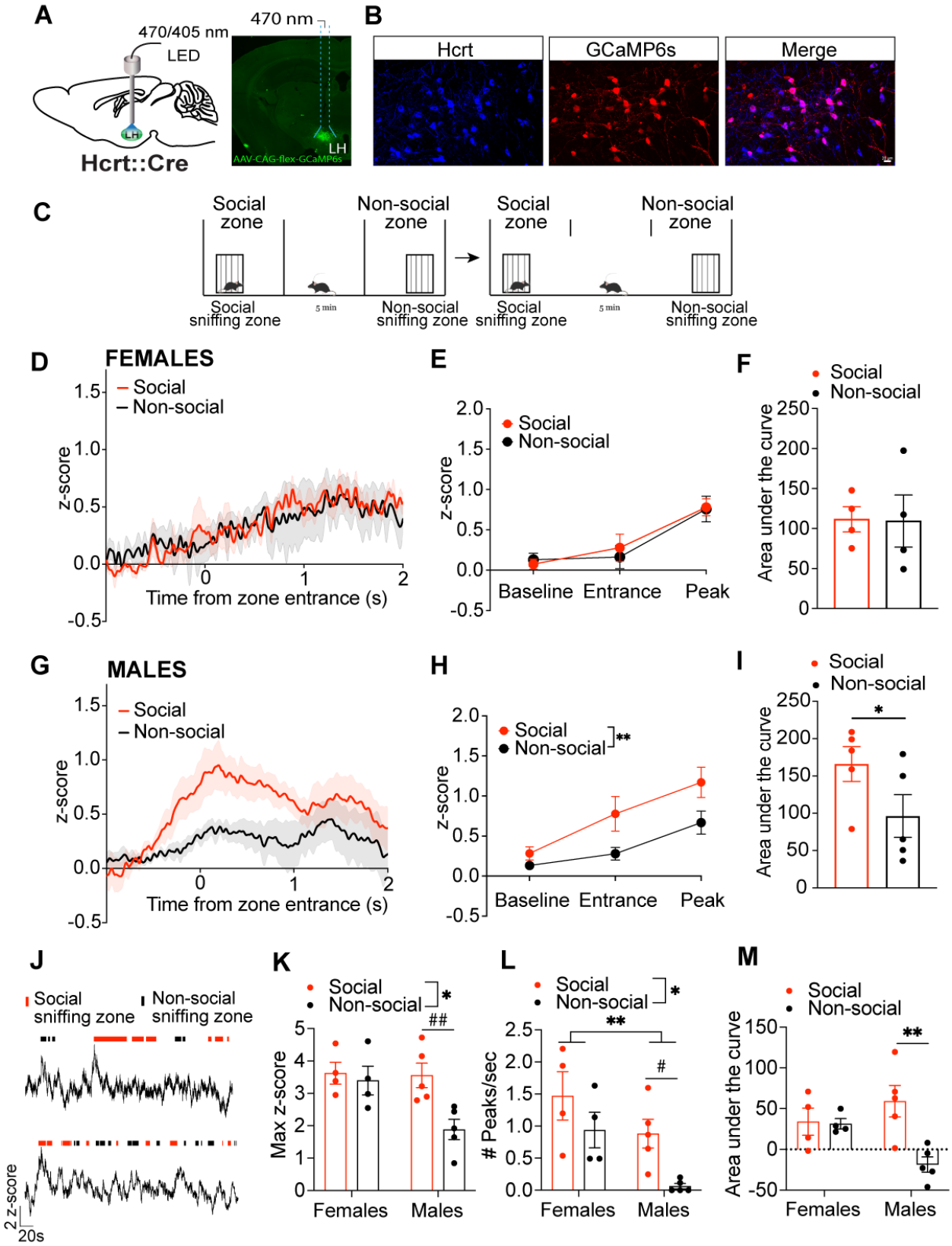
A
470/405 nm
LED
470 nm
LH
AAV-CAG-flex-GCaMP6s
Hcrt::Cre
B
Hcrt
GCaMP6s
Merge
C
Social zone
Non-social zone
Social sniffing zone
5 min
Non-social sniffing zone
D
FEMALES
Social
Non-social
z-score
Time from zone entrance (s)
E
Baseline
Entrance
Peak
F
Area under the curve
G
MALES
H
I
J
Social sniffing zone
Non-social sniffing zone
2 z-score
20s
K
Max z-score
Females
Males
L
Peaks/sec
M

Figure 2

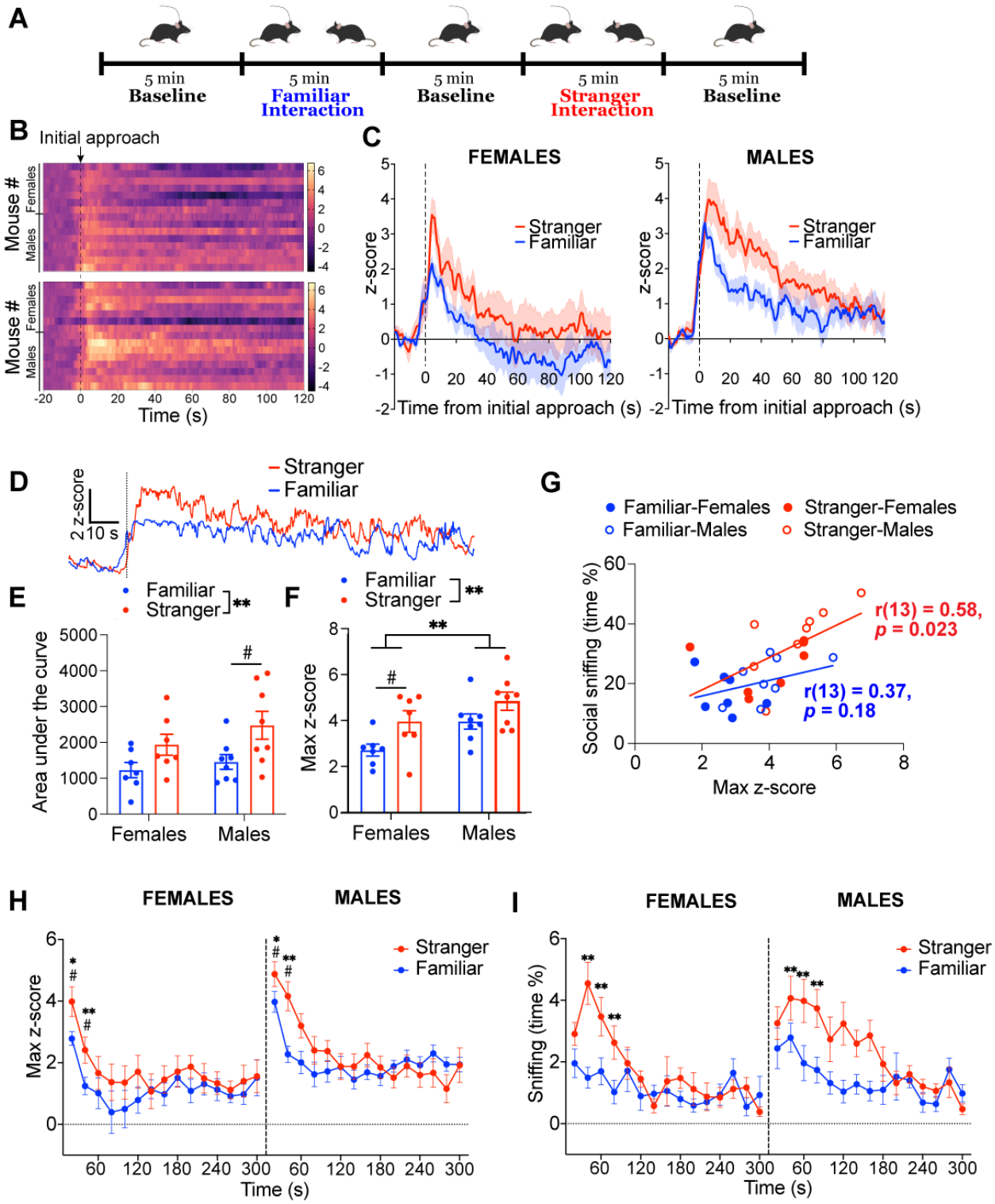
A
5 min
Baseline
5 min
Familiar
Interaction
5 min
Baseline
5 min
Stranger
Interaction
5 min
Baseline
B
Initial approach
Mouse #
Females
Males
Time (s)
C
FEMALES
MALES
Stranger
Familiar
z-score
Time from initial approach (s)
D
Stranger
Familiar
2 z-score
10 s
E
Familiar
Stranger
Area under the curve
Females
Males
F
Familiar
Stranger
Max z-score
Females
Males
G
Familiar-Females
Stranger-Females
Familiar-Males
Stranger-Males
Social sniffing (time %)
Max z-score
r(13) = 0.58,
p = 0.023
r(13) = 0.37,
p = 0.18
H
FEMALES
MALES
Stranger
Familiar
Max z-score
Time (s)
I
FEMALES
MALES
Stranger
Familiar
Sniffing (time %)
Time (s)

Figure 3

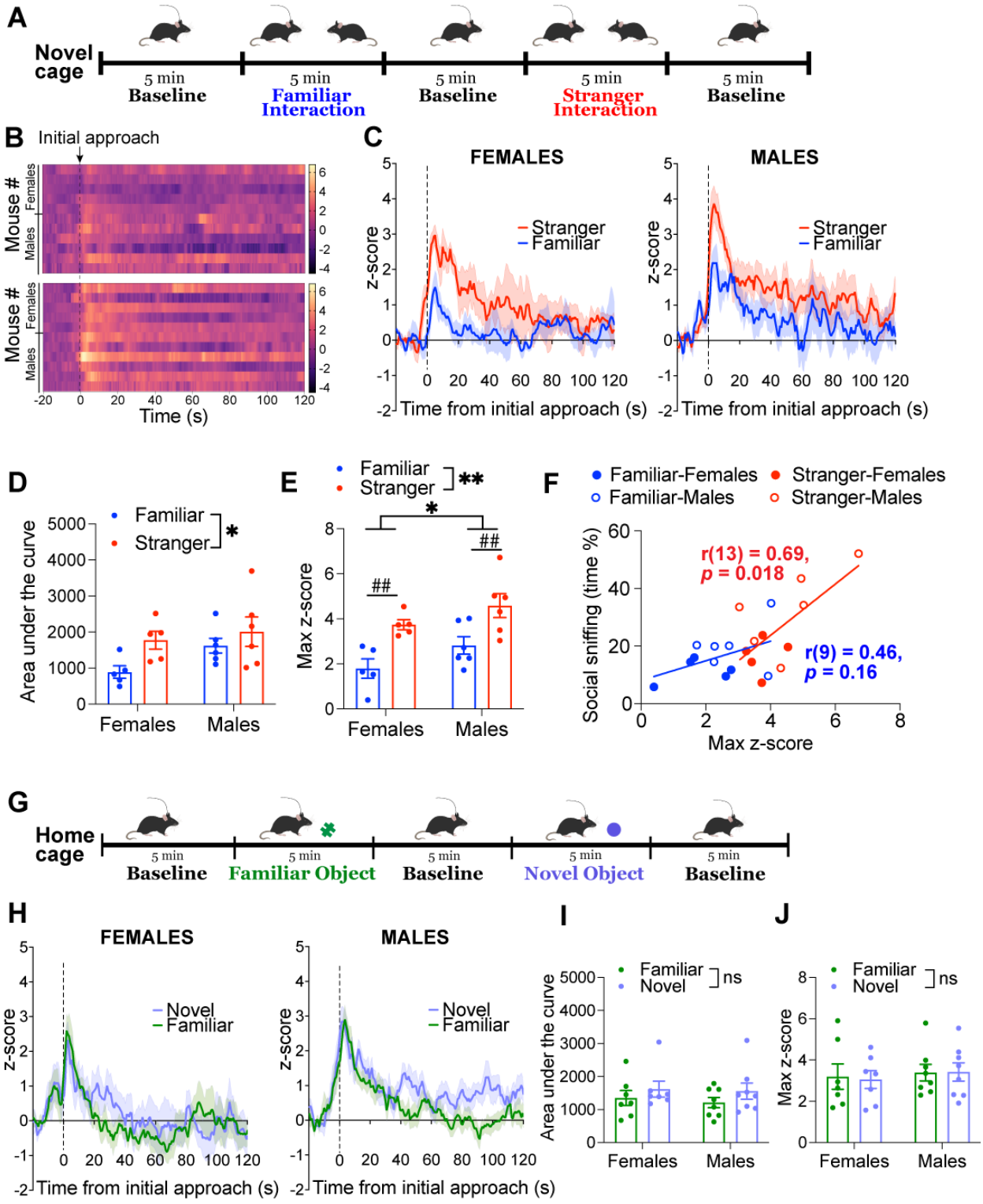
A
Novel cage
5 min Baseline
5 min Familiar Interaction
5 min Baseline
5 min Stranger Interaction
5 min Baseline
B
Initial approach
Mouse #
Females
Males
Time (s)
C
FEMALES
MALES
Stranger
Familiar
z-score
Time from initial approach (s)
D
Familiar
Stranger
Area under the curve
Females
Males
E
Max z-score
F
Familiar-Females
Stranger-Females
Familiar-Males
Stranger-Males
Social sniffing (time %)
r(13) = 0.69, p = 0.018
r(9) = 0.46, p = 0.16
Max z-score
G
Home cage
5 min Baseline
5 min Familiar Object
5 min Baseline
5 min Novel Object
5 min Baseline
H
FEMALES
MALES
Novel
Familiar
z-score
Time from initial approach (s)
I
Area under the curve
ns
J
Max z-score
ns

Figure 4

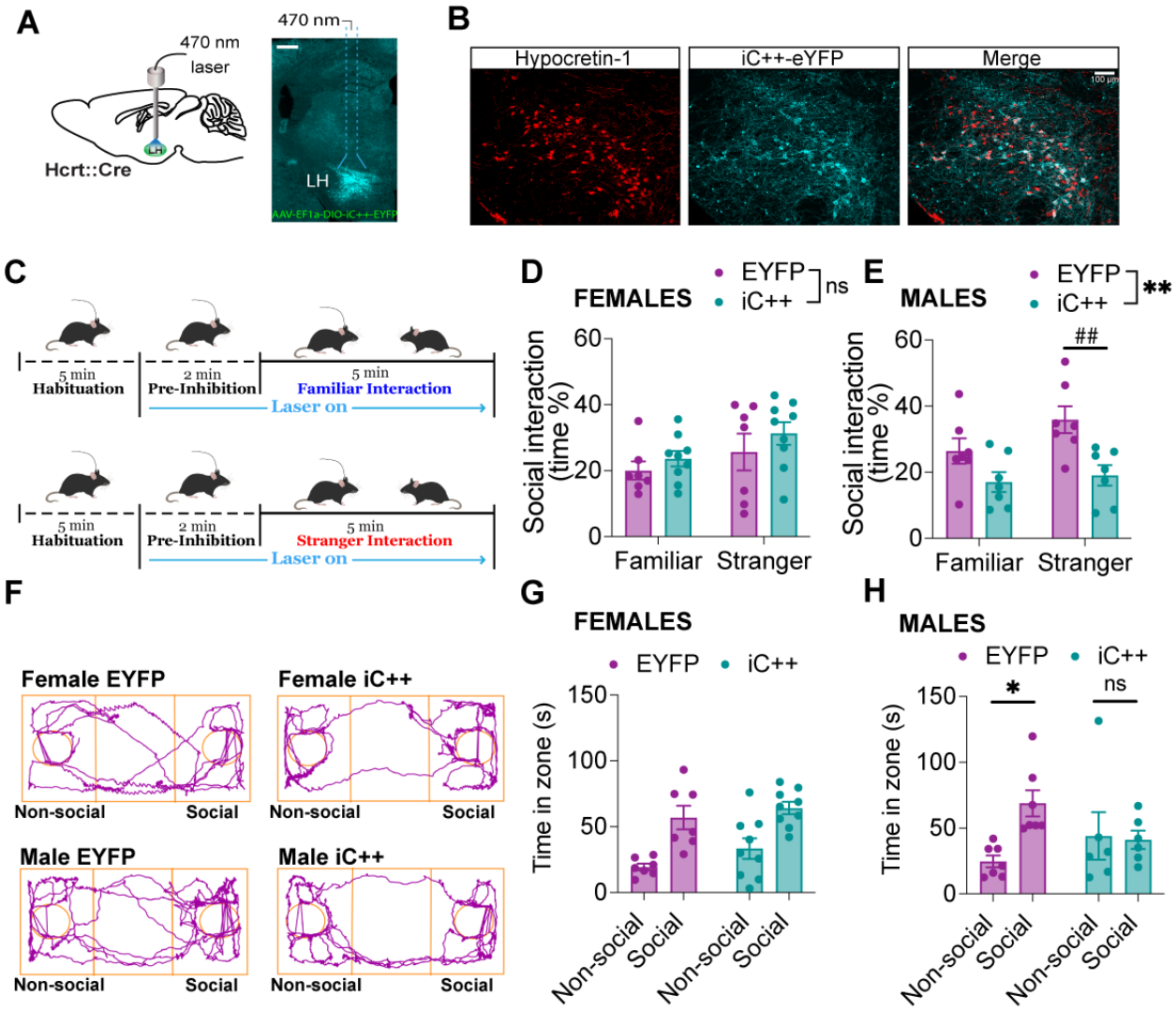
A
470 nm
laser
LH
Hcrt::Cre
470 nm
LH
AAV-EF1a-DIO-iC++-EYFP
B
Hypocretin-1
iC++-eYFP
Merge
100 µm
C
5 min
Habituation
2 min
Pre-Inhibition
5 min
Familiar Interaction
Laser on
5 min
Habituation
2 min
Pre-Inhibition
5 min
Stranger Interaction
Laser on
D
FEMALES
EYFP
iC++
ns
Social interaction (time %)
60
40
20
0
Familiar
Stranger
E
MALES
EYFP
iC++
**
##
Social interaction (time %)
60
40
20
0
Familiar
Stranger
F
Female EYFP
Non-social
Social
Female iC++
Non-social
Social
Male EYFP
Non-social
Social
Male iC++
Non-social
Social
G
FEMALES
EYFP
iC++
Time in zone (s)
150
100
50
0
Non-social
Social
Non-social
Social
H
MALES
EYFP
iC++
*
ns
Time in zone (s)
150
100
50
0
Non-social
Social
Non-social
Social

Figure 5

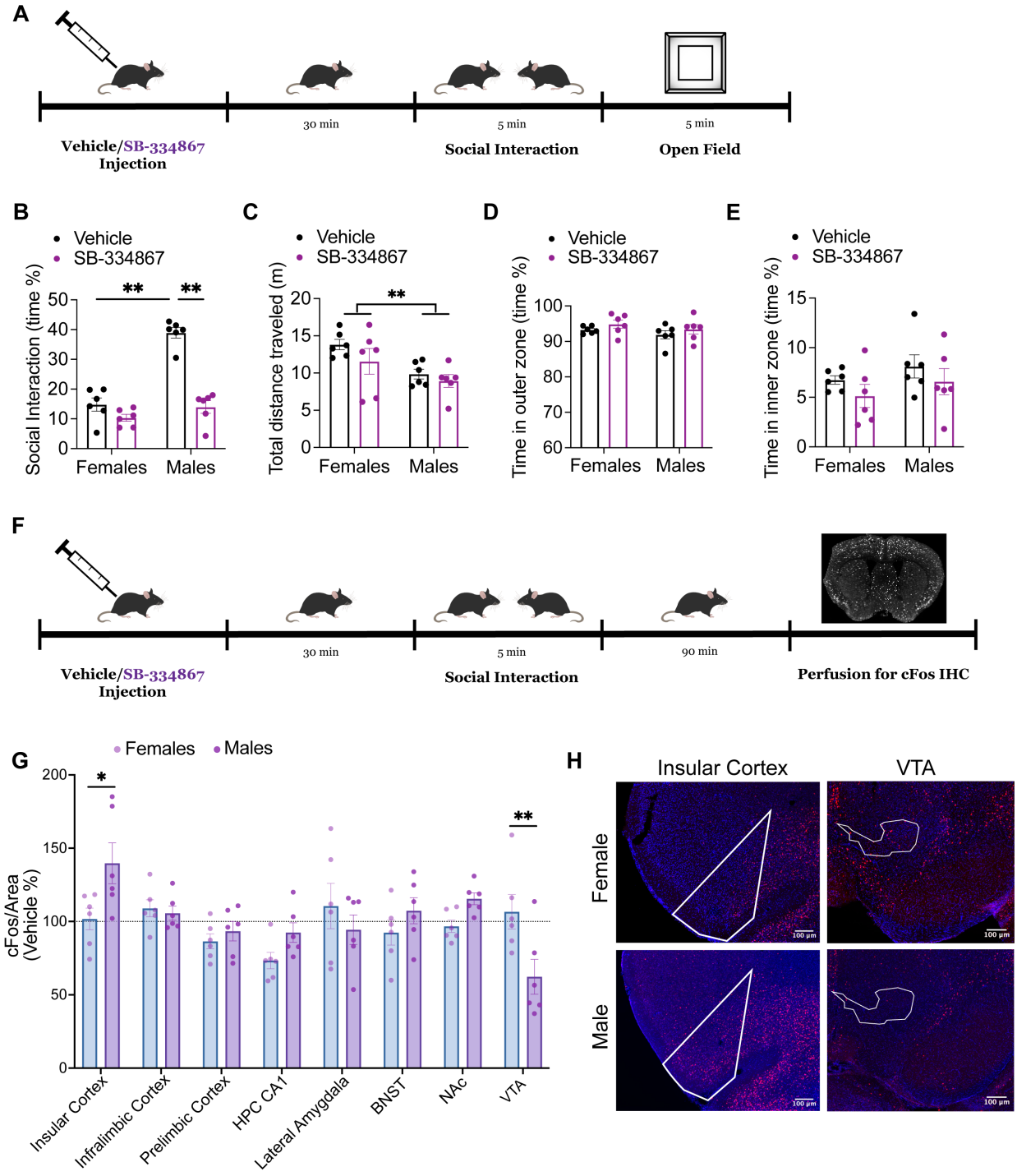
A
30 min
5 min
5 min
Vehicle/SB-334867 Injection
Social Interaction
Open Field
B
Vehicle
SB-334867
Social Interaction (time %)
Females
Males
C
Total distance traveled (m)
D
Time in outer zone (time %)
E
Time in inner zone (time %)
F
30 min
5 min
90 min
Vehicle/SB-334867 Injection
Social Interaction
Perfusion for cFos IHC
G
Females
Males
cFos/Area (Vehicle %)
Insular Cortex
Infralimbic Cortex
Prelimbic Cortex
HPC CA1
Lateral Amygdala
BNST
NAc
VTA
H
Insular Cortex
VTA
Female
Male